The effect of composition on chlorine solubility and behaviour in silicate melts

Word count 6610 excluding abstract and references

Richard W Thomas[1] (richard.thomas@earth.ox.ac.uk)

Bernard J Wood[1] (bernie.wood@earth.ox.ac.uk)

[1]Department of Earth Sciences, University of Oxford, South Parks Road, Oxford OX1 3AN, UK

REVISION2

This is the peer-reviewed, final accepted version for American Mineralogist, published by the Mineralogical Society of America.
The published version is subject to change. Cite as Authors (Year) Title. American Mineralogist, in press.
DOI: https://doi.org/10.2138/am-2022-8450. http://www.minsocam.org/

Abstract

We have performed experiments at 1.5 GPa and 1400 ^{o}C on 25 different bulk compositions to determine the effects of major element compositions on the Cl contents of silicate melts at known fugacities of Cl_2 and O_2. The experimental method involved mixing a "sliding" Cl buffer, a mixture of AgCl, AgI and Ag with the silicate bulk composition and performing the experiment in a graphite capsule together with a source of CO_2 ($AgCO_3$). The graphite capsules were sealed inside welded Pt tubes in order to maintain a CO_2-CO atmosphere with oxygen fugacity fixed at the C-CO-CO_2 (CCO) buffer. During the experiment, the Cl buffer segregates leaving a Cl-bearing melt, which quenches to a glass. We used the results to define chloride capacity C_{Cl} for each melt at the pressure and temperature of the experiment:

$$C_{Cl} = \frac{Cl\ (wt\%)}{\sqrt{f(Cl_2)}} \times \sqrt[4]{f(O_2)}$$

Chloride capacity was found to correlate positively with optical basicity and NBO/T and negatively with ionic porosity and the Larsen Index. We combined our new data with the results of Thomas and Wood (2021) to derive an equation describing the composition, pressure and temperature dependence of the chloride capacity:

$$logC_{Cl} = 1.601 + (4470X_{Ca} - 3430X_{Si} + 2592X_{Fe} - 4092X_{K}\text{-}894\text{P})/\text{T}$$

In this equation, X_{Ca}, X_{Si} and so on refer to the oxide mole fractions on a single cation basis, P is in GPa and T in K. The equation reproduces 58 data points with an r^2 of 0.96 and a standard error of 0.089. The addition of literature data on hydrous experiments indicates that the effects of <4.3 weight% H_2O are small enough to be ignored. We also performed experiments aimed at determining the conditions of NaCl saturation in melts. When combined with literature data we obtained:

This is the peer-reviewed, final accepted version for American Mineralogist, published by the Mineralogical Society of America.
The published version is subject to change. Cite as Authors (Year) Title. American Mineralogist, in press.
DOI: https://doi.org/10.2138/am-2022-8450. http://www.minsocam.org/

$$log(Cl^-) = log(a_{NaCl}) + 0.06 - (2431X_{Ca} + 3430X_{Si} - 2592X_{Fe} + 3484X_{Na} + 4092X_K - 2417)/T$$

Where (Cl^-) is the Cl content of the melt in weight % a_{NaCl} is the activity of NaCl (liquid) and the other symbols are the same as before. The results indicate that basalt dissolves approximately 8 times more Cl than rhyolite at a given NaCl activity i.e., Cl is approximately 8 times more soluble in basalt than in rhyolite.

Key Words: basalt; rhyolite; Cl solubility in melts; Compositional effects on Cl solubility; Cl degassing; Chloride capacity; NaCl saturation in melts

INTRODUCTION

The volatile components whose behaviour is best understood in silicate melts are H_2O and CO_2 (Symonds et al. 1994; De Vivo et al. 2005). In the case of H_2O, the reasons are its high abundance, the major effects it has on viscosity, the melting and crystallisation temperatures of melts, and its importance in hydrothermal ore deposition associated with igneous activity. CO_2 came to be studied experimentally in the 1970's initially because of the observation that carbonatites were magmas with origins in the mantle. More recently concerns about volcanogenic CO_2 as a greenhouse gas has facilitated the establishment of a good database to describe CO_2 solubility in a wide range of melts over a wide range of physical conditions (Brooker et al. 2001; Stanley et al. 2011), allowing for the development of robust models, such as *VolatileCalc* (Newman and Lowenstern 2002) and *MagmaSat* (Ghiorso and Gualda 2 2015).

A third group of elements that are geologically and environmentally important and

whose behaviour in melts requires further elucidation are the halogens. Chlorine, the second most abundant of the halogens (after F) in both the primitive and depleted mantle, and in the bulk continental crust (Pyle and Mather2009), is an important ligand in hydrothermal processes and plays a major role in transporting economically important metals such as Au and Cu in solution (Blundy et al. 2015). The segregation of Cl-rich brines from melts in the later stages of igneous activity can lead to significant metal transport and has resulted in major economic deposits at, for example, Broken Hill in New South Wales, Australia (Millsteed and Mavrogenes 2015) and in porphyry copper deposits (Nash 1976; Fuge et al. 1986). Moore and Nash (1974) found that halite rich fluid inclusions perfectly outlined the Cu-rich ore zone at Bingham Canyon, Utah, USA and that fluid inclusions found in a PGE deposit helped delineate the ore at the Stillwater Complex, Montana USA (Hanley et al. 2008). Lastly, the two most economically important iron oxide copper-gold (IOCG) deposits in Chile, Mantoverde, and Candelaria-Punta del Cobre, both exhibit high-salinity fluid inclusions (Marschik and Kendrick 2015).

Halogens released by volcanism act to transport trace metals in gaseous form into the environment (Scholtysik and Canil 2021), which act as catalysts for the destruction of stratospheric ozone (von Glasow et al. 2009) and in some cases can cause major local environmental degradation. The 1783 eruption of Laki, for example, led to the release of ~8 million tonnes of F causing the deaths by fluorosis of a large fraction of Iceland's sheep and cattle population and about 25% of the population in the ensuing famine.

During differentiation of igneous melts, the halogens behave as highly incompatible elements (Edmonds et al. 2009; Pyle and Mather 2009) where they are concentrated in the melts until lost in a gas or fluid phase or incorporated into a quenched glass and minor crystalline phases such as apatite or sodalite (Sharp and Draper 2013). Thermodynamic equilibrium speciation calculations and observations of modern volcanic edifices (Symonds

et al. 1992; Martin et al. 2006) indicate that the halogens are predominantly degassed in the form of halogen-bearing acids (HF, HCl, HBr, and HI; Gerlach, (2004); Martin et al. (2006)). Volcanic gases typically comprise > 90% H_2O plus CO_2, with < 10% SO_2 plus HCl and HF and trace amounts of H_2S, H_2, CO, HBr, and HI (Pyle and Mather 2009; Martin et al. 2012). Estimates of halogen fluxes vary greatly and current volcanic degassing from arc and non-arc eruptions are estimated to vary from 0.3 Tg/Yr to 5.5 Tg/Yr for HCl, 0.15 Tg/Yr to 0.58 Tg/Yr for HF, 0.0001Tg/Yr to 0.016 Tg/Yr for HBr, and 0.00004 Tg/Yr to 0.0017Tg/Yr for HI (Gerlach 2004; Aiuppa et al. 2009; Pyle and Mather 2009; Webster et al. 2018).

Given their environmental and geochemical importance, the properties and distribution of halogens in natural and experimentally produced silicate melts and coexisting fluid phases are the subject of broad ongoing interest. They are observed to have profound effects on the phase equilibria and viscosities of melts (Zimova and Webb 2006; Filiberto and Treiman 2009; Baasner et al. 2013) leading, for example, to Cl being twice as effective on a molar basis at lowering the liquidus of basalt as H_2O (Filiberto and Treiman 2009). Experimental determinations under controlled conditions show that Cl solubility tends to increase with decreasing SiO_2 concentration in the melt (Iwasaki and Katsura, 1967; Carroll and Webster, 1994; Webster et al. 1999; Signorelli and Carroll 2000; Webster and De Vivo 2002). Decreases in the SiO_2 concentration generally correlates with increasing concentrations of network-modifying cations. Experiments employing saturation in hydro-saline liquids (Webster et al. 2015) indicate that the Cl concentration increases at fixed temperature and pressure with increasing CaO, MgO, and alkali contents of the silicate melts.**{{auth: ok?}OK}** The compositional effects were parameterised as a Cl solubility model (Webster et al. 2015), which provides an important baseline for future work. This model has some uncertainty, however, because the coexisting hydrosaline liquids change in composition, and hence the Cl_2 fugacity, as the silicate melt composition changes. A method

105 by which Cl fugacity can be varied independently of the silicate melt composition is
106 required to better constrain the compositional effects on Cl solubility. Thomas and Wood,
107 (2021) developed such a method based on the equilibrium:

108 $$AgCl = 2Ag + Cl_2. \quad (1)$$
109 liquid liquid

110 Coexistence of liquid AgCl and liquid Ag metal at fixed pressure and temperature buffer the
111 fugacity of Cl_2. Since Ag is virtually insoluble in silicate melt, except under very oxidising
112 conditions (Thomas and Wood 2021), the composition of a coexisting silicate melt can be
113 varied almost at will at a known, (in principle), buffered, Cl fugacity. In practice, we found
114 that Cl fugacities were so high using the Ag/AgCl buffer that discrete Ca-Mg chloride
115 liquids segregated from haplobasaltic melts at the experimental conditions of 1.5
116 GPa/1400^{o}C. In order to suppress the exsolution of chlorides, we therefore, diluted the AgCl
117 with AgI to form a mixed halide with a known ratio of Cl to I. This approach enables the Cl
118 fugacity to be calculated from a combination of the thermodynamic data for equilibrium (1),
119 the volumes of the liquid Ag and AgCl, and the ratio of Cl/(Cl+I) in the "sliding" Ag/AgCl-
120 AgI buffer. We have tested similar approaches with AgF, AgBr, and AgI and can report that
121 all three can be treated in a similar manner to AgCl in order to fix the fugacities of F, Br,
122 and I respectively. Given its abundance and importance in hydrothermal fluids and volcanic
123 gases, however, the remainder of this report will be dedicated to the behaviour of Cl in
124 silicate melts.

125 Thomas and Wood, (2021) used the Ag/AgCl buffer method described above to
126 investigate the nature of the initial dissolution of Cl in two silicate melts, an Icelandic basalt
127 and a haplobasalt of composition $An_{50}Di_{28}Fo_{22}$ (Table 1). We found that, at 1.5 GPa/1400
128 °C, dissolution of Cl follows Henry's Law with the Cl concentration proportional to the

This is the peer-reviewed, final accepted version for American Mineralogist, published by the Mineralogical Society of America.
The published version is subject to change. Cite as Authors (Year) Title. American Mineralogist, in press.
DOI: https://doi.org/10.2138/am-2022-8450. http://www.minsocam.org/

129 square root of Cl fugacity and the fourth root of oxygen fugacity up to concentrations of at
130 least 1.6 wt% Cl in the basalt and 2.6 wt% Cl in the haplobasalt. These observations imply
131 that $2Cl^-$ ions in the melt replace O^{2-} according to the reaction:

132 $$Cl_2 + [O^{2-}]_{melt} = 2[Cl^-]_{melt} + \frac{1}{2}O_2$$

133 ((2))

134 The Cl^- ions in the melt are dissociated from one another and it is straightforward to show
135 that, at equilibrium, the concentration of Cl^- in the melt is proportional to $f_{Cl_2}^{0.5}$ and inversely
136 proportional to $f_{O_2}^{0.25}$. At concentrations greater than 2.6 wt% Cl in the haplobasalt and ~1.6
137 wt% Cl in the natural basalt, the relationship between Cl concentration and $f_{Cl_2}^{0.5}$ deviates in a
138 direction consistent with the mutual avoidance of the Cl^- ions i.e., the concentration increases
139 less strongly with increasing $f_{Cl_2}^{0.5}$ than in the Henry's Law region (Fig. 1).

140 Our observation that a Ca-rich composition ($An_{50}Di_{28}Fo_{22}$) dissolves substantially
141 more Cl at fixed $f(Cl_2)$ than basalt (Thomas and Wood 2021) is qualitatively in agreement
142 with the model of Webster et al (2015), which incorporates a strong positive correlation
143 between CaO and MgO concentrations in the melt and the Cl content in the melt. These
144 correlations also appear to be reflected in the X-ray absorption (Evans et al. 2008; McKeown
145 et al. 2011) and Nuclear Magnetic Resonance spectra (Stebbins and Du 2002; Sandland et al.
146 2004) of Cl in quenched glasses. These authors concluded that Cl nearest-neighbours, and
147 hence the strongest influences on Cl solubility, are predominantly Ca and Mg (Evans et al.
148 2008; McKeown et al. 2011) or a combination of alkaline and alkali cations (Stebbins and Du
149 2002; Sandland et al. 2004).

150 From the preceding discussion and Figure 1, it is clear that there are strong
151 compositional dependences of Cl solubility in a silicate melt and that the CaO, MgO, and

Na_2O concentrations probably play major roles. Our aim here is to quantify these compositional effects at known Cl fugacity in order to extend the application of our Cl fugacity buffer and to build on the experimental approach of Webster et al. (2015). A major advantage of the buffer method is that it is applicable to anhydrous melts, which enables us to study compositional effects in the absence of H_2O and a coexisting hydrous fluid.

EXPERIMENTAL METHODOLOGY

Starting compositions

Since the principal aim of this study was to determine compositional effects on Cl solubility we used a wide range of starting compositions comprising 7 natural samples, and 18 synthetic compositions. (Table 1). Synthetic starting compositions were prepared from mixtures of analytical grade oxide powders, (with Fe added as Fe_2O_3), and carbonate powders (Na_2CO_3, $CaCO_3$, and K_2CO_3). Powders were ground under ethanol for a minimum of 2.5 hours to ensure homogeneity. The mixtures were subsequently pressed into pellets, decarbonated by incremental heating overnight from 400 to 800 °C, and the Fe reduced overnight in a 1-atmosphere furnace at 1100 °C and at an $f(O_2)$ of IW+1 using a CO-CO_2 gas mixture. The reduced mixes were used as starting materials for the experiments. A small fraction of each was re-ground into powder and then melted at 1400 °C in air at 1 atm to check the starting composition (Table 1).

Controlling Cl and oxygen fugacity

Chlorine fugacity was controlled by intimately mixing AgI and AgCl in a 75:25 ratio. The presence of iodine reduces the Cl fugacity enough such that blebs of $CaCl_2$ and $MgCl_2$ do

not segregate from the silicate glass, therefore ensuring that the starting composition remains constant. The Cl fugacity is then obtained from Thomas and Wood (2021):

$$logf(Cl_2) = -\frac{11440}{T} + 2.961 + \frac{2150P}{T} - \frac{208P^2}{T} + 2log\left(\frac{Cl}{Cl+I}\right)_{halide} - 2log\left(\frac{Ag}{Ag+Pt}\right)_{metal} \quad ((3))$$

In equation (3) the ratios (Cl/(Cl+I)) and (Ag/(Ag+Pt)) refer respectively to the mole fractions of Cl in the mixed halide melt and Ag in the coexisting liquid metal. Mixing in both liquids was assumed to obey Raoult's Law; an assumption, which can be readily shown to be reasonable for AgCl-AgI liquids based on the temperature and position of the 1 atmosphere eutectic (Levin et al. 1964), and to be reasonable for Ag-Pt liquids which are Ag-rich (generally > 0.8 mole fraction; Table 2).

The starting silicate compositions were ground together with the AgI/AgCl mixture in a ratio of 75:25 (and packed into 2.5mm outside diameter, 1 mm inside diameter graphite capsules. The graphite capsules were placed, with a 1 mm graphite lid, inside 3mm outside diameter Pt capsules with mixtures of graphite and Ag_2CO_3 above and below the graphite capsule. The platinum capsule was welded shut. During the experiment, the Ag_2CO_3 decomposes to Ag liquid metal, and, by reaction with graphite, CO_2. The coexistence of C and CO_2 buffers oxygen fugacity at CCO (Jakobsson and Oskarsson, 1994):

$$logf(O_2)_{(CCO)} = 4.325 - \left(\frac{21803}{T}\right) + 0.171\left(\frac{(P-1)}{T}\right) \quad ()(4) \ (4)$$

At the conditions employed in this study (1400 °C and 1.5 GPa), the log$f$(O_2) is fixed by this assembly at -7.17 (Thomas and Wood 2021). The experiments employed a 32 mm long, 12.5 mm outside diameter, 8 mm inside diameter Ca fluoride cylinder as the principal pressure medium. Inside this cylinder was an 8 mm O.D., 6 mm I.D. graphite cylinder which acts as the furnace. The 3 mm outside diameter capsule was placed in the centre of the graphite

198 furnace with crushable MgO pieces above, below and around the capsule. All experiments
199 were then performed with an end-loaded 'Boyd and England'-type ½ inch piston-cylinder
200 apparatus (Boyd and England, 1960) housed at the University of Oxford. The temperature
201 was measured and controlled using an alumina-sheathed C-type ($W_{95}Re_5$–$W_{74}Re_{26}$)
202 thermocouple, introduced through a hole in the upper MgO piece and separated from the
203 capsule by a 0.5 mm thick alumina disc. All experimental assembly pieces were heated to
204 minimise the presence of water as much as possible to ensure anhydrous conditions. This
205 included heating the MgO pieces at 1000 °C overnight.

206 Experiments were performed at a constant temperature and pressure of 1400 °C and
207 1.5 GPa, respectively (Table 2) using the *'hot piston-in'* method and the pressure calibrations
208 of McDade et al. (2002). In order to test for approach to equilibrium, Thomas and Wood,
209 (2021) performed a time series of experiments from 5 min to 2 h at 1400 °C and 1.5 GPa
210 using a haplobasaltic composition with the oxygen fugacity fixed at the CCO buffer and the
211 Cl fugacity given by an initial AgI:AgCl ratio of 75:25 by weight. We found negligible
212 change in Cl concentration between 5 mins and 2 hours indicating a rapid approach to
213 equilibrium. We repeated the test in our new study using a more viscous dacitic composition
214 (Table 1), which might be expected to equilibrate more slowly than basalt. As before,
215 however, the concentration of Cl was, within uncertainty, unchanged in experiments from 5
216 min to 2 hours duration with a range of 0.46 – 0.50 wt% (Table 2). Subsequent experiments
217 were therefore performed for 1 h or more (Table 2).

218 All experiments resulted in a clear segregation of the silicate glass, metal halide and
219 metal (Figure 2). All experiments were quenched by cutting the power to the graphite furnace
220 (cooling at ≈120 °C/s). Once extracted, the recovered capsule was cleaned and weighed to
221 ensure no mass was lost or gained during the experiment.

Two additional experiments were performed with the aim of determining the Cl content of melt at NaCl saturation. For these experiments, we used a natural phonolite (Table 1; LS-17985) as the silicate, intimately mixed with 20 wt% NaCl. One experiment was buffered at the CCO oxygen buffer as described above and the other at the Re-ReO_2 buffer using the assembly described by Thomas and Wood (2021). The experiments were held at 1100 °C and 1.0 GPa for 2 hours and quenched in the usual manner.

Analytical techniques

During the experiment, the buffer-silicate mixture segregates into a homogeneous translucent glass, a metal chloride/iodide phase and an Ag-rich metal alloy (Figure 2). The NaCl-buffered experiments segregated distinctive blobs of NaCl which could be analysed easily with the electron microprobe. The capsules were mounted in epoxy, ground to expose a cross section of the charge and polished with water-free diamond paste, using isopropanol as a lubricant to prevent any Cl loss (Mungall and Brenan 2003).

Product silicate glasses and Cl fugacity buffers were analysed on the CAMECA SX-Five-FE field emission electron microprobe at the University of Oxford's Department of Earth Sciences. A 20 nA beam current, 15 kV accelerating voltage, and a defocused 10 μm beam diameter was used for the glass analyses. To minimise the potential for element migration during analysis, Cl, Na, K, and Si were analysed first. Standards used for silicate glass analysis were natural albite (Si, Al, Na), andradite (Ca, Fe), synthetic thallium bromoiodide (Br,I) **{{AU: Please ask the authors to fully explain "Tl(Br.I)".DB}}** (I), TiO_2 (Ti), Manganese (Mn), Sanidine (K), synthetic periclase (Mg), NaCl crystals (Cl), Ag, and Pt. Counting times were a minimum of 30 s peak and 15 s background for all elements, except for Cl, which was 80 s peak and 40 s background. The latter gave a detection limit of ≤ 100 ppm for Cl. For Na and K we used 20s peak and 10s background counting times to

reduce the chance of element migration from the beam and these elements were analysed first on 2 different spectrometers. Replicate analyses on the same spots of glass revealed that the Cl counts were stable and consistent under these conditions. Over 20 points were taken on each silicate portion of the charge, and 10 to 20 points were taken on the remaining buffer and resultant metal phases. Results remained consistent with a low (< 0.2 wt%) standard deviation (Table 2). Secondary standards including Durango apatite, which contains a known Cl concentration of 0.41 wt% (Kusebauch et al. 2015) were used to ensure accurate Cl analysis. We obtained an average of 0.412 wt% Cl with a standard deviation of 0.013% for 84 analyses.

RESULTS

All experiments, except those at NaCl saturation, were performed at 1400 °C and 1.5 GPa, using the CCO buffer ($f(O_2)$ = -7.17 log units). All run conditions, the Cl concentrations in the resultant glass phases, and the calculated Cl fugacities are given in Table 2. Complete analyses of the silicate glass products are presented in supplementary Table S1. In order to compare the results obtained at different Cl fugacities, and, considering that Cl solubility is proportional to the Henry's Law relationship derived from reaction (2), we define the *chloride capacity* (C_{Cl}; Table 2) as:

$$C_{Cl} = \frac{Cl\ (wt\%)}{\sqrt{f(Cl_2)}} \times \sqrt[4]{f(O_2)} \quad ((5))$$

We calculated the ferric-ferrous ratio of each experiment using the equation of Kress and Carmichael (1991) and adjusted the FeO and Fe_2O_3 contents of our products accordingly.

Henry's Law and melt composition

Figure 3 shows the Cl contents of melts of a wide range of compositions equilibrated at different fugacities of Cl with oxygen fugacity controlled at the CCO buffer and temperature and pressure of 1400 °C and 1.5 GPa respectively. As can be seen, Cl dissolution in all seven melts follows Henry's Law to concentrations of between, depending on major element composition, at least 0.5 wt% (dacite) and 2.6 wt % ($An_{50}Di_{28}Fo_{22}$) Cl. The effect of composition is dramatic with more than an order of magnitude difference between Cl contents (under constant $f(O_2)$, $f(Cl_2)$ conditions) of a low SiO_2, high CaO haplobasalt, which is rich in Cl and a high SiO_2, low CaO dacite, poor in Cl. Specific compositional effects will be discussed further below.

Correlation of empirical compositional parameters with chloride capacity

There are a number of empirical parameters which have been proposed as being simple ways of representing the complexities of silicate melt compositions by a single parameter. These are all basically ways of representing the degree of polymerisation of the melt by assigning different roles to "network-forming" (e.g., SiO_2) and "network-modifying" or depolymerising (e.g., Na_2O) oxide components. Since Cl is observed to replace oxygen in the silicate matrix, it is logical to assume that chloride capacity is a function of the way in which oxygen is bonded in the silicate melt.

Optical basicity: Optical basicity is a parameter which empirically allocates an electron donor power (Lewis basicity) to each individual oxide in a silicate melt matrix (Banin et al. 1997). Optical basicity, denoted, Λ, was proposed as a useful index of melt properties by Duffy and Ingram (1971) and adapted by Duffy and Ingram (1976) and Duffy (2004) as follows:

This is the peer-reviewed, final accepted version for American Mineralogist, published by the Mineralogical Society of America.
The published version is subject to change. Cite as Authors (Year) Title. American Mineralogist, in press.
DOI: https://doi.org/10.2138/am-2022-8450. http://www.minsocam.org/

294 $$\Lambda = \frac{\sum X_i n_i \Lambda_i}{\sum X_i n_i}$$

295 ((6))

296 In equation (6) X_i is the mole fraction of oxide i, n_i is the number of oxygen atoms of the
297 oxide, and Λ_i is the optical basicity of oxide i. As expected, optical basicity decreases with
298 increasing SiO_2 and Al_2O_3 contents and increases with CaO, MgO, and alkali concentrations.
299 Therefore, as anticipated from Figure 3, there is a strong positive correlation of chloride
300 capacity with optical basicity (Fig 4a).

301

302 *NBO/T:* A second empirical way of representing the properties of the oxygen atoms in a
303 silicate matrix is through the ratio of non-bridging oxygens to tetrahedrally coordinated
304 cations, NBO/T. The chemical rationale is that oxygen atoms which bridge between
305 tetrahedral Si and Al have different properties from those which terminate silicate chains or
306 are present in isolated tetrahedra. We calculated NBO/T following the approach of Mills
307 (1993). This derives Y_{NB} and X_T as follows for $Fe^{3+}/(Fe^{2+}+Fe^{3+}) < 0.3$ (Mills 1993) from the
308 mole fractions x of the different oxides:

309 $$Y_{NB} = \sum 2[xCaO + xMgO + xFeO + xMnO + xNa_2O + xK_2O] + 6xFe_2O_3 -$$

310 $$2xAl_2O_3$$((7))

311 $$X_T = \sum xSiO_2 + xTiO_2 + 2xP_2O_5 + 2xAl_2O_3$$

312 ((8))

313 $$\frac{NBO}{T} = \frac{Y_{NB}}{X_T}$$

314 ((9))

This is the peer-reviewed, final accepted version for American Mineralogist, published by the Mineralogical Society of America.
The published version is subject to change. Cite as Authors (Year) Title. American Mineralogist, in press.
DOI: https://doi.org/10.2138/am-2022-8450. http://www.minsocam.org/

315 Since Y_{NB} increases with CaO, MgO and alkali contents, NBO/T correlates positively with
316 optical basicity and chloride capacity as shown in Figure 4b.

317

318 *Ionic porosity:* This parameter is a calculation of the percentage of the melt volume
319 unoccupied by cations and anions and defined as (Dowty, 1980):

320 $$Z = 100(1 - V_{ca}/V_L)$$

321 ((10))

322 In equation (10) V_{ca} is the total volume occupied by constituent atoms (cations + anions) in
323 one gram of melt, and V_L is the melt volume (cm^3/g) calculated using the oxide partial molar
324 volumes as given by Lange and Carmichael (1987). We calculated the ionic porosity of each
325 product glass using the calculator presented in Iacono-Marziano et al. (2010). Their model
326 uses the parameters of Carroll and Stolper, (1993) with volumes of individual cations and
327 anions calculated from effective ionic radii given by (Shannon and Prewitt, 1969; Shannon,
328 1976), assuming spherical geometry. All melt compositions were recalculated to 100% before
329 calculating ionic porosity. Since ionic porosity generally decreases with increasing Ca, Mg,
330 and alkalis and increases with SiO_2, chloride capacity correlates negatively with ionic
331 porosity (Fig. 4c).

332

333 *Larsen Index:* The Larsen index is a measure of the extent of differentiation of a melt,
334 defined as follows (Larsen, 1938):

335 $$LI = \left[\left(\frac{1}{3}SiO_2 + K_2O\right) - \left((FeO + \frac{9}{10}Fe_2O_3 + MnO) + CaO + MgO\right)\right] \quad (11)$$

336 This index (Fig 4d) has been used extensively to correlate Cl solubility with chemical
337 composition (e.g. Webster et al. 2009; Webster et al. 2015; Webster et al. 2018; Webster et

al. 2019). Given the positive term in SiO_2 and negative term in CaO, chloride capacity correlates, as expected, negatively with the Larsen Index as shown in Figure 4d.

Oxide mole fractions: It is clear from Figure 4 and the preceding discussion that all of the empirical compositional parameters considered provide reasonable descriptions of the compositional dependence of chloride capacity over the broad compositional range investigated. We were seeking, however, to identify subtle variations in chloride capacity due to different cations of similar, but not identical chemical behaviour. We therefore fitted the logarithm of the chloride capacity using SPSS software to compositional terms for each of the constituent oxides, with each oxide recalculated as the mole fraction on a single cation basis. We used stepwise linear regression applying the F-test (α=0.05) to determine which compositional parameters are significant. In order to ensure that the compositional terms approach zero at infinite temperature, the oxide mole fractions were divided by temperature. Terms that were not significant at an F of 0.05 were excluded. This approach resulted in the following equation:

$$log C_{Cl} = 1.601 + (4470X_{Ca} - 3430X_{Si} + 2592X_{Fe} - 4092X_{K}\text{-}894\text{P})/\text{T} \quad (12)$$

R^2=0.96; standard error = 0.089

Surprisingly, in view of previous results and inferences (Stebbins and Du 2002; Sandland et al. 2004; Evans et al. 2008; McKeown et al. 2011), our data do not require terms for Mg and Na contents. The influences of these cations have plausibly been subsumed into the terms for Ca, Si, and K. In order to take account of pressure and temperature effects on chloride capacity we regressed the data together with the data from Thomas and Wood, (2021) in which the pressure and temperature effects on chloride capacity for the $An_{50}Di_{28}Fo_{22}$ composition and the Icelandic basalt were independently established. As before

we found that the term in reciprocal temperature is insignificant, and that the P/T term is required. The value of the latter in equation **{{auth: ok?}OK like this }**(12) is within uncertainty of the same terms previously obtained by regression and is close to the value expected for the replacement of O^{2-} by 2 Cl^{-} (Thomas and Wood 2021). A spreadsheet enabling the calculation of Cl fugacities and chloride capacitites as defined in equations (12) and (15) is provided as the electronic supplement, *'ChlorCalc_v1'*.

DISCUSSION

The effects of H_2O on chloride capacity

There are a considerable number of studies of the partitioning of Cl and other elements between silicate melts and aqueous fluids (Shinohara et al. 1989; Métrich and Rutherford, 1992; Webster, 1992; Kravchuk and Keppler, 1994; Webster and Rebbert, 1998; Bureau et al. 2000; Signorelli and Carroll 2000; Signorelli and Carroll 2002; Botcharnikov et al. 2007; Chevychelov et al. 2008; Stelling et al. 2008; Alletti et al. 2009; Webster et al. 2009; Zajacz et al. 2012; Alletti et al. 2014; Beermann et al. 2015; Botcharnikov et al. 2015). In general, however, because of the difficulties of fluid separation and analysis, authors calculate the composition of the fluid by mass balance from the starting composition and the measured melt composition. This approach works reasonably well for Cl, but concentrations of charge-balancing cations in the fluid are difficult to estimate. This is important because for experiments performed at fixed $f(O_2)$ or fixed $f(H_2)$, the Cl_2 fugacity is related to the HCl fugacity via the equilibria:

$$H_2O = 0.5\,O_2 + H_2 \quad (13)$$

$$H_2 + Cl_2 = 2\,HCl \quad (14)$$

If the concentrations of charge balancing cations, such as Na, Ca, and K are known, then any Cl in excess of charge balance can be allocated, approximately, to HCl. If only Cl is known, however, the fugacity of HCl must either be calculated by allocating all Cl to HCl or by arbitrarily subtracting some fraction of the Cl as "bonded with other cations" in the fluid.

Bearing in mind these difficulties we attempted to incorporate the effects of H_2O on chloride capacities using melt-aqueous fluid Cl partitioning data on a phonolite at 1000 °C and 10-250 MPa (Alletti et al. 2014). In this case, the authors have calculated the Cl content of the fluid as HCl. For the experiments of Alletti et al. (2014) we used the Modified Redlich Kwong equation of state for H_2O-H_2-HCl fluids with parameters for H_2O, H_2 (Holloway, 1977), and HCl (Prausnitz et al. 1999). This enabled us to calculate the Cl_2 fugacity of each experiment using the equilibrium constant for equilibria (13) and (14) from the NIST-JANAF thermochemical tables (https://janaf.nist.gov/).

Adding the 23 data points from Alletti et al. (2014) to our 62 data points and performing a stepwise linear regression with the same approach as before we obtained:

$$logC_{Cl} = 0.571 + (4873X_{Ca} - 3803X_{Si} + 2724X_{Fe} + 1891\text{-}\ 943\text{P})/\text{T} \qquad (15)$$

R^2=0.94; standard error = 0.117

The important points to note are as follows: 1) Although we added the H_2O contents (0.6-4.3 wt%) in mole fractions (0.04-0.26) as a parameter to the regression, the term in H_2O was not significant at the α=0.05 level. 2) The X_{Ca}, X_{Si}, X_{Fe}, and P/T terms are very similar in equations (12) and (15) implying that they are quite robust. 3) The temperature range of the data has been extended by a further 200 °C, which has required the introduction of a term in 1/T. **{{AU: The authors need to provide further discussion of this sentence. I see no difference in the 1/T terms in Equations 12 and 15. D.B.}Don has misread the equations. (12) and (15) have almost identical P/T terms, but (15) has the term 1891/T and no such term is present in (12).}** The latter was found to be not significant in our earlier study, presumably because of the more restricted temperature range employed in our higher-pressure experiments.

Although other data in the literature have the potential to provide additional compositional constraints, we have found it difficult to treat all studies in a consistent way. We therefore present equation (15) as an illustration of the extension of our approach to lower temperatures and moderate H_2O contents (up to 4.3%) on the understanding that a

414 systematic addition of H_2O to experiments using our buffering approach is required to better
415 resolve the question of the effects of H_2O on chloride capacity.

416

417 ## IMPLICATIONS

418 ### H_2O and HCl degassing

419 Thomas and Wood, (2021) observed that Cl should not degas significantly as HCl
420 during ascent of basalt until pressures are well below 10 MPa, and that most Cl would be
421 degassed below 2 MPa, equivalent to ~ 80 meters depth. In Figure 5 we illustrate the effect of
422 composition on these estimates made by assuming that the evolved gas is dominantly H_2O.
423 We considered 4 melts, basalt, andesite, dacite, and rhyolite (anhydrous compositions in
424 Table 1) and estimated their dry liquidi at 50 MPa using *alphaMELTS for Python*
425 (Antoshechkina and Ghiorso 2018). We then calculated the H_2O content of each melt at 50
426 MPa and a temperature just above the dry liquidus (1220, 1200, 1080 and 1030 $^{\circ}$C for basalt,
427 andesite, dacite, and rhyolite respectively) using a spreadsheet from Moore et al. (1998). The
428 latter yields saturated H_2O contents of between 2.13 (andesite) and 2.34 (rhyolite) weight% at
429 50 MPa (Table 3).

430 In order to calculate the degassing path of Cl from the melts of interest, we estimated
431 their chloride capacities from equation (15) at an oxygen fugacity corresponding to the
432 fayalite-magnetite–quartz (FMQ) buffer, assumed H_2O saturation at 50 MPa, and applied
433 starting concentrations of 2000 ppm (0.2 wt%) Cl in all 4 melts. We then calculated the
434 amounts of H_2O and the dominant chloride species, HCl (Shinohara et al. 1989), degassed in
435 H_2O-HCl fluids from 50 to 0.1 MPa in 0.5 MPa intervals. Although, as before, we adopted
436 the Modified Redlich Kwong (MRK) equation of state for the H_2O-H_2-HCl gas phase,
437 fugacity coefficients for H_2 and HCl in the water-rich gas are so close to 1.0 that they could

This is the peer-reviewed, final accepted version for American Mineralogist, published by the Mineralogical Society of America.
The published version is subject to change. Cite as Authors (Year) Title. American Mineralogist, in press.
DOI: https://doi.org/10.2138/am-2022-8450. http://www.minsocam.org/

438 have been assumed to be perfect gases with little change in the result.

439 It should be noted that, although the chloride capacity depends on $f(O_2)$, the degassing
440 of HCl is actually independent of oxygen fugacity. This can be seen by combining the
441 dissolution reaction of Cl in the melt with those for the dissociation of H_2O and formation of
442 HCl:

443 $$Cl_2 + [O^{2-}]_{melt} = 2[Cl^-]_{melt} + \frac{1}{2}O_2 \quad (16a)$$

444 $$H_2O = H_2 + \frac{1}{2}O_2 \quad (16b)$$

445 $$2HCl = H_2 + Cl_2 \quad (16c)$$

446 If we subtract reaction (16b) from (16a) and add (16c) we eliminate oxygen and Cl fugacities
447 and obtain:

448 $$2HCl + [O^{2-}]_{melt} = 2[Cl^-]_{melt} + H_2O \quad (16d)$$

449 Thus, the results shown in Figure 5 are independent of the oxygen fugacity provided that Cl
450 is dominantly degassed as HCl, which is the case in low pressure, high temperature
451 environments.

452 As can be seen in Figure 5, and anticipated from equation (15), the effects of Ca, Fe,
453 and Si on chloride capacity result in basaltic melts having much higher Cl solubilities and
454 lower tendences to degas HCl than silica-rich melts poor in Ca and Fe. We calculate that a
455 basaltic melt containing 2000 ppm (0.2 wt%) Cl at 50 MPa will degas only 0.03 wt% Cl
456 during the ascent to the surface. In contrast, andesitic, dacitic, and rhyolitic melts, initially
457 containing 0.2 wt% Cl, should degas 0.08, 0.12, and 0.17 wt % respectively during ascent.
458 Almost half of the degassing takes place at pressures below 3 MPa (110 meters depth),
459 conditions under which the gas pressure would be expected to fluctuate substantially due to
460 melt migration and convection. The calculations therefore show that HCl would degas mainly

in the very uppermost parts of a volcanic edifice or during an eruption. This conclusion is consistent with the observations of Saito et al. (2005) at Miyekejima Volcano, Japan, who found that Cl remains in the melt, even after shallow degassing, and thus only degasses at very low pressures, well after H_2O and CO_2 (Spilliaert et al. 2006). More recently, Edmonds et al. (2009) placed constraints on the depths of Cl degassing at Kilauea, and found that Cl degasses at depths of 35 meters or less, at pressures below 1 MPa, and below pressures of sulfur degassing. This conclusion coincides with the findings of (Lesne et al. 2011) who performed experiments to simulate decompression-driven, closed-system degassing of basaltic magma in equilibrium with an H-C-O-S-Cl fluid. They found that dissolved Cl displayed minimal loss to the fluid over a wide pressure range, remaining in the melt from 400 MPa to 25 MPa. Finally, the enrichment of Cl in thermal springs is also believed to reflect Cl degassing at very shallow conditions (Li et al. 2015).

NaCl activities in Cl-containing silicate melts

Brine separation from melts is an important process in the generation of many economically important ore deposits (Cline and Bodnar 1994; Bruce et al. 1999; Bortnikov 2006; Gleeson and Turner 2007; Wilkinson 2013; Blundy et al. 2015; Nshimiyimana et al. 2015; Essarraj et al. 2016; Blundy et al. 2021). Understanding of the depths at which saturation occurs is fundamental to the development of an understanding of the process in specific environments.

In order to provide a basis for understanding brine saturation, Webster and De Vivo, (2002) and Webster et al. (2015) performed experiments in which silicate melts of a wide range of compositions were saturated with chloride-rich liquids, the latter being dominated by NaCl and KCl. In some cases, hydrous chlorides such as $FeCl_2.4H_2O$ and $CaCl_2.2H_2O$ were added instead of, or in addition to, NaCl and KCl, as was oxalic acid, as a source of H_2O and

This is the peer-reviewed, final accepted version for American Mineralogist, published by the Mineralogical Society of America.
The published version is subject to change. Cite as Authors (Year) Title. American Mineralogist, in press.
DOI: https://doi.org/10.2138/am-2022-8450. http://www.minsocam.org/

485 CO_2, as well as $PtCl_4$. Importantly, the experimental products were very close to chloride
486 saturation and Webster et al. (2015) used the results to model the solubility of chloride in
487 silicate melts.

488 In order to connect our chloride capacity measurements to the chloride saturation
489 experiments of Webster and De Vivo, (2002) and Webster et al. (2015), we performed two
490 experiments at 1100 °C and 1.0 GPa in which a phonolitic melt was saturated in NaCl at two
491 different oxygen fugacities. In these cases, the activity of NaCl is 1.0 at 1100°C/1 GPa while
492 the earlier experiments, performed at 1 bar to 0.7 GPa and 700 to 1250 °C, were saturated in
493 liquids with significantly lower, but unknown NaCl activities. The important consideration is,
494 however, that comparison of our data with the earlier results of Webster and De Vivo, (2002)
495 and Webster et al. (2015) should be based on NaCl activities as close to 1.0 as possible. We
496 therefore excluded all of the earlier experiments in which Cl was added as $PtCl_4$ and those in
497 which H_2O and/or Ca and Mg chlorides were added. This left 100 experiments of Webster
498 and De Vivo, (2002) and Webster et al. (2015) in which Cl was added as NaCl and KCl and
499 in which the NaCl activity was high.

500 The experimental data were considered in terms of the equilibrium:

501 $$2NaCl + [O^{2-}]_{melt} = 2[Cl^{-}]_{melt} + Na_2O$$

502 liquid NaCl melt (17)

503 We rearrange the equilibrium constant for equation ((17)) to yield:

504 $$log\left(\frac{a_{Cl^- melt}}{a_{O^{2-}melt}^{0.5}}\right) = log(a_{NaCl}) - 0.5\log\left(a_{Na_2O}\right) + 0.5logK \quad (18)$$

505 The term on the left-hand side is directly related to the chloride capacity through equilibrium
506 (2). It must therefore have the same compositional dependence on the chloride capacity as
507 that derived from equations (12) or (15). We therefore used equation (12) and calculated an

This is the peer-reviewed, final accepted version for American Mineralogist, published by the Mineralogical Society of America.
The published version is subject to change. Cite as Authors (Year) Title. American Mineralogist, in press.
DOI: https://doi.org/10.2138/am-2022-8450. http://www.minsocam.org/

"effective" activity ratio $\left(\frac{a_{Cl^-melt}}{a_{O^{2-}melt}^{0.5}}\right)$ from the Cl concentration (Cl^-) in wt % and oxide mole fractions on a single cation basis :

$$log\left(\frac{a_{Cl^-melt}}{a_{O^{2-}melt}^{0.5}}\right) = log(Cl^-) - (4470X_{Ca} - 3430X_{Si} + 2592X_{Fe} - 4092X_K)/\mathrm{T} \quad (19)$$

In equation (19) Cl^- denotes the wt% concentration of Cl in the melt and the compositional terms on the right-hand side remove the compositional dependence of $\left(\frac{a_{Cl^-melt}}{a_{O^{2-}melt}^{0.5}}\right)$ as described by equation (12). This gave us 102 data points of known values of pressure, temperature, and the left-hand side of equation (18). **{{AU: Please query the authors as to whether they mean 18 or 19 at this point. D.B. We do mean (18)}}** Using the standard state for NaCl as pure liquid NaCl at the pressure and temperature of interest, we assumed that the activity of NaCl in our NaCl-saturated experiments was 1.0 and that the data of Webster and De Vivo (2002) and Webster et al. (2015) referred to slightly lower activity values of 0.8. We believe that the latter is a reasonable assumption since NaCl activity values of about 0.5 fitted less well with our data for which the NaCl activity is known. We then regressed $log(a_{NaCl}) - log\left(\frac{a_{Cl^-melt}}{a_{O^{2-}melt}^{0.5}}\right)$ against 1/T, P/T, and oxide mole fractions as before in order to obtain the compositional dependence of NaCl saturation. The activity of Na_2O (equation 18) is combined with the composition, temperature, and pressure terms. Using stepwise linear regression and applying the F-test as before we obtained:

$$log(a_{NaCl}) - log\left(\frac{a_{Cl^-melt}}{a_{O^{2-}melt}^{0.5}}\right) = -0.06 + (6901X_{Ca} + 3484X_{Na} - 2417)/\mathrm{T} \quad (20)$$

The standard error of the fit is 0.124 and $r^2 = 0.85$. We can now put (19) and (20) together to obtain the Cl content of the melt at any NaCl activity as follows:

528 $$log(Cl^-) = log(a_{NaCl}) + 0.06 - (2431X_{Ca} + 3430X_{Si} - 2592X_{Fe} + 3484X_{Na} +$$

529 $$4092X_K - 2417)/T \qquad ((21))$$

530 It is interesting to note that the Cl content should not depend on oxygen fugacity $f(O_2)$ at
531 NaCl saturation as indicated by equation (17). We confirmed this supposition by performing
532 experiments at both the Re/ReO_2 (4 log $f(O_2)$ units above CCO) and the CCO buffers from
533 which Cl contents of 1.09 and 1.00 wt%, respectively were obtained (Table 2).

534 Figure 6 shows the calculated Cl contents of the same 4 melts as in Figure 5 plotted as
535 a function of NaCl activity. The form of equation (21) imposes a linear relationship between
536 NaCl activity and Cl content, but as can be seen, the major element composition has an
537 appreciable effect on NaCl solubility and saturation in natural silicate melts. Thus, for
538 example, we calculate that at 200 MPa and 900 °C, the basalt will contain 3.6% Cl (possibly
539 metastably) at NaCl saturation (activity = 1.0) while the rhyolite will reach NaCl saturation at
540 0.45 weight % Cl. The latter figure is similar to values measured in melt inclusions from
541 some felsic magmas (Webster et al, 2020) indicating that NaCl-rich brines are much more
542 likely to separate from felsic than from basic magmas. Equation (21), therefore, leads to a
543 means of using the compositions of melts to estimate the compositions of coexisting fluids,
544 specifically their NaCl contents at the conditions of fluid separation. In this we follow the
545 example of Webster et al. (2020) who used melt inclusion data from a large number of
546 localities to estimate whether or not the melts were in equilibrium with a hydrosaline liquid.

547 # ACKNOWLEDGEMENTS

548 We acknowledge the stimulation and guidance provided by Jim Webster's numerous papers
549 on halogen behaviour in silicate melts. RWT is grateful to the National Environmental
550 Research Council, and the Oxford Doctoral Training Partnership in Environmental Research
551 for studentship and funding (NE/L002612/1). BJW acknowledges funding from Science and

Technology Facilities Council grant ST/R000999/1 and the NERC FAMOS project NE/P017452/1. We would like to thank Paula Antoschechkina of Caltech for advice in using AlphaMELTS. We acknowledge the thorough reviews of Bruno Scaillet and an anonymous reviewer, and discussions with Jon Blundy. Further thanks are owed to Dan Harlov as editor.

REFERENCES CITED

558 Aiuppa, A., Baker, D.R., and Webster, J.D. (2009) Halogens in volcanic systems. Chemical
559 Geology 263, 1–18.

560 Alletti, M., Baker, D.R., Scaillet, B., Aiuppa, A., Moretti, R., and Ottolini, L. (2009) Chlorine
561 partitioning between a basaltic melt and H 2 O–CO 2 fluids at Mount Etna. Chemical
562 Geology 263, 37–50.

563 Alletti, M., Burgisser, A., Scaillet, B., and Oppenheimer, C. (2014) Chloride partitioning and
564 solubility in hydrous phonolites from Erebus volcano: A contribution towards a multi-
565 component degassing model. GeoResJ, 3–4 27–45.

566 Antoshechkina, P.M., and Ghiorso, M.S. (2018) MELTS for MATLAB : A new educational
567 and research tool for computational p. Abstract #ED44B-23. American Geophysical
568 Union, Fall Meeting 2018.

569 Baasner, A., Schmidt, B.C., and Webb, S.L. (2013) The effect of chlorine, fluorine and water
570 on the viscosity of aluminosilicate melts. Chemical Geology, 357, 134–149.

571 Banin, A., Hah, F.X., Kan, I., and Cieelsky, A. (1997) Acidic volatiles and the Mars soil.
572 Journal of Geophysical Research, 102, 13341–13356.

573 Beermann, O., Botcharnikov, R.E., and Nowak, M. (2015) Partitioning of sulfur and chlorine
574 between aqueous fluid and basaltic melt at 1050°C, 100 and 200 MPa. Chemical
575 Geology, 418, 132–157.

576 Blundy, J., Mavrogenes, J., Tattitch, B., Sparks, S., and Gilmer, A. (2015) Generation of
577 porphyry copper deposits by gas-brine reaction in volcanic arcs. Nature Geoscience, 8
578 235–240.

579 Blundy, J., Afanasyev, A., Tattitch, B., Sparks, S., Melnik, O., Utkin, I., and Rust, A. (2021)
580 The economic potential of metalliferous sub-volcanic brines. Royal Society Open

581 Science, 8.

582 Bortnikov, N.S. (2006) Geochemistry and origin of the ore-forming fluids in hydrothermal-
583 magmatic systems in tectonically active zones. Geology of Ore Deposits, 48, 3–28.

584 Botcharnikov, R.E., Holtz, F., and Beherens, H. (2007) The effect of CO2 on the solubility of
585 H2O-Cl fluids in andesitic melt. European Journal of Mineralogy, 19, 671–680.

586 Botcharnikov, R.E., Holtz, F., and Behrens, H. (2015) Solubility and fluid–melt partitioning
587 of H2O and Cl in andesitic magmas as a function of pressure between 50 and 500 MPa.
588 Chemical Geology, 418, 117–131.

589 Boyd, F.R., and England, J.L. (1960) Apparatus for phase-equilibrium measurements at
590 pressures up to 50 kilobars and temperatures up to 1750°C. Journal of Geophysical
591 Research, 65, 741–748.

592 Brooker, R.A., Kohn, S.C., Holloway, J.R., and McMillan, P.F. (2001) Structural controls on
593 the solubility of CO2 in silicate melts part I: Bulk solubility data. Chemical Geology,
594 174 225–239.

595 Bruce, S., Yardley, B.W.D., Banks, D., Boyce, A.J., Munoz, M., Courjault-Rade, P., and
596 Tollon, F. (1999) The genesis of mineralising brines in the South West Massif Central,
597 France. Mineral Deposits: Processes to Processing, Vols 1 and 2, 62A 29–32.

598 Bureau, H., Keppler, H., and Métrich, N. (2000) Volcanic degassing of bromine and iodine:
599 Experimental fluid/melt partitioning data and applications to stratospheric chemistry.
600 Earth and Planetary Science Letters, 183, 51–60.

601 Carroll, M.R., and Stolper, E.M. (1993) Noble gas solubilities in silicate melts and glasses:
602 New experimental results for argon and the relationship between solubility and ionic
603 porosity. Geochimica et Cosmochimica Acta, 57, 5039–5051.

Carroll, M.R., and Webster, J.D. (1994) Solubilities of sulfur, noble gases, nitrogen, chlorine, and fluorine in magmas. Mineralogical Society of America Reviews in Mineralogy, 30 231 –279.

Chevychelov, V., Bocharnikov, R.E., and Holtz, F. (2008) Experimental study of chlorine and fluorine partitioning between fluid and subalkaline basaltic melt. Doklady Earth Sciences, 422, 93–97.

Cline, J.S., and Bodnar, R.J. (1994) Direct evolution of brine from a crystallizing silicic melt at the Questa, New Mexico, Molybdenum deposit. Economic Geology, 89, 1780–1802.

De Vivo, B., Lima, A., and Webster, J.D. (2005) Volatiles in volcanic systems. Elements, 1, 19–24.

Dowty, E. (1980) Crystal-chemical factors affecting the mobility of ions in minerals. American Mineralogist, 65, 174–182.

Duffy, J.A. (2004) Relationship between optical basicity and thermochemistry of silicates. Journal of Physical Chemistry B, 108, 7641–7645.

Duffy, J.A., and Ingram, M.D. (1971) Establishment of an optical scale for Lewis basicity in inorganic oxyacids, molten salts, and glasses. Journal of the American Chemical Society, 93, 6448–6454.

——— (1976) An interpretation of glass chemistry in terms of the optical basicity concept. Journal of Non-Crystalline Solids 21, 373–410.

Edmonds, M., Gerlach, T.M., and Herd, R.A. (2009) Halogen degassing during ascent and eruption of water-poor basaltic magma. Chemical Geology 263, 122–130.

Essarraj, S., Boiron, M.-C., Cathelineau, M., Tarantola, A., Leisen, M., Boulvais, P., and Maacha, L. (2016) Basinal brines at the origin of the Imiter Ag-Hg deposit (Anti-Atlas,

627 Morocco): Evidence from LA-ICP-MS data on fluid inclusions, halogen signatures, and
628 stable isotopes (H, C, O). Economic Geology, 111, 1753–1781.

629 Evans, K.A., Mavrogenes, J.A., O'Neill, H.S., Keller, N.S., and Jang, L.Y. (2008) A
630 preliminary investigation of chlorine XANES in silicate glasses. Geochemistry,
631 Geophysics, Geosystems, 9, 1–15.

632 Filiberto, J., and Treiman, A.H. (2009) The effect of chlorine on the liquidus of basalt: First
633 results and implications for basalt genesis on Mars and Earth. Chemical Geology 263,
634 60–68.

635 Fuge, R., Andrews, M.J., and Johnson, C.C. (1986) Chlorine and iodine, potential pathfinder
636 elements in exploration geochemistry. Applied Geochemistry, 1, 111–116.

637 Fusswinkel, T., Wagner, T., Wälle, M., Wenzel, T., Heinrich, C.A., and Markl, G. (2013)
638 Fluid mixing forms basement-hosted Pb-Zn deposits: Insight from metal and halogen
639 geochemistry of individual fluid inclusions. Geology, 41, 679–682.

640 Gerlach, T.M. (2004) Volcanic sources of tropospheric ozone-depleting trace gases.
641 Geochemistry, Geophysics, Geosystems, 5, 1–16.

642 Ghiorso, M.S., and Gualda, G.A.R. (2015) An H2O–CO2 mixed fluid saturation model
643 compatible with rhyolite-MELTS. Contributions to Mineralogy and Petrology, 169, 53.

644 Gleeson, S.A., and Turner, W.A. (2007) Fluid inclusion constraints on the origin of the brines
645 responsible for Pb-Zn mineralization at Pine Point and coarse non-saddle and saddle
646 dolomite formation in southern Northwest Territories. Geofluids, 7, 51–68.

647 Hanley, J.J., Mungall, J.E., Pettke, T., Spooner, E.T.C., and Bray, C.J. (2008) Fluid and
648 halide melt Inclusions of magmatic origin in the ultramafic and lower banded series,
649 stillwater complex, Montana, USA. Journal of Petrology, 49, 1133–1160.

650 Holloway, J.R. (1977) Fugacity and activity of molecular species in supercritical fluids. In
651 Fraser D.G. (eds) Thermodynamics in Geology. NATO Advanced Study Institutes
652 Series (Series C — Mathematical and Physical Sciences), vol 30. Springer, Dordrecht.

653 Iacono-Marziano, G., Paonita, A., Rizzo, A., Scaillet, B., and Gaillard, F. (2010) Noble gas
654 solubilities in silicate melts: New experimental results and a comprehensive model of
655 the effects of liquid composition, temperature and pressure. Chemical Geology 279,
656 145–157.

657 Iwasaki, B., and Katsura, T. (1967) The solubility of hydrogen chloride in volcanic rock
658 melts at a total pressure of one atmosphere and at temperatures of 1200°C and 1290°C
659 under anhydrous conditions. Bulletin of the Chemical Society of Japan, 40, 554–561.

660 Jakobsson, S., and Oskarsson, N. (1994) The system C-O in equilibrium with graphite at high
661 pressure and temperature: An experimental study. Geochimica et Cosmochimica Acta,
662 58, 9–17.

663 Johnson, L.H., Burgess, R., Turner, G., Milledge, H.J., and Harris, J.W. (2000) Noble gas and
664 halogen geochemistry of mantle fluids: Comparison of African and Canadian diamonds.
665 Geochimica et Cosmochimica Acta, 64, 717–732.

666 Kravchuk, I.F., and Keppler, H. (1994) Distribution of chloride between aqueous fluids and
667 felsic melts at 2 kbar and 800°C. European Journal of Mineralogy, 6, 913–924.

668 Kusebauch, C., John, T., Whitehouse, M.J., Klemme, S., and Putnis, A. (2015) Distribution
669 of halogens between fluid and apatite during fluid-mediated replacement processes.
670 Geochimica et Cosmochimica Acta, 170 225–246.

671 Lange, R.A., and Carmichael, I.S.E. (1987) Densities of Na2O-K2O-CaO-MgO-FeO-Fe2O3-
672 Al2O3-TiO2-SiO2 liquids: New measurements and derivated partial molar properties.

673 Geochimica et Cosmochimica Acta, 51 2931–2946.

674 Larsen, E.S. (1938) Some new variation diagrams for groups of igneous rocks. The Journal of
675 Geology, 46, 505–520.

676 Lesne, P., Kohn, S.C., Blundy, J., Witham, F., Botcharnikov, R.E., and Behrens, H. (2011)
677 Experimental simulation of closed-system degassing in the system basalt-H2O-CO2-S-
678 Cl. Journal of Petrology, 52, 1737–1762.

679 Levin, E.M., Robbins, C.R., and McMurdie, H.F. (1964) Phase diagrams for ceramists.
680 American Ceramic Society, Columbus, Ohio.

681 Li, L., Bonifacie, M., Aubaud, C., Crispi, O., Dessert, C., and Agrinier, P. (2015) Chlorine
682 isotopes of thermal springs in arc volcanoes for tracing shallow magmatic activity. Earth
683 and Planetary Science Letters, 413, 101–110.

684 Marschik, R., and Kendrick, M.A. (2015) Noble gas and halogen constraints on fluid sources
685 in iron oxide-copper-gold mineralization: Mantoverde and La Candelaria, Northern
686 Chile. Mineralium Deposita, 50, 357–371.

687 Martin, R.S., Mather, T.A., and Pyle, D.M. (2006) High-temperature mixtures of magmatic
688 and atmospheric gases. Geochemistry, Geophysics, Geosystems, 7, 1–14.

689 Martin, R.S., Wheeler, J.C., Ilyinskaya, E., Braban, C.F., and Oppenheimer, C. (2012) The
690 uptake of halogen (HF, HCl, HBr and HI) and nitric (HNO3) acids into acidic sulphate
691 particles in quiescent volcanic plumes. Chemical Geology 296–297, 19–25.

692 McDade, P., Wood, B.J., Van Westrenen, W., Brooker, R., Gudmundsson, G., Soulard, H.,
693 Najorka, J., and Blundy, J. (2002) Pressure corrections for a selection of piston-cylinder
694 cell assemblies. Mineralogical Magazine, 66, 1021–1028.

695 McKeown, D.A., Gan, H., Pegg, I.L., Stolte, W.C., and Demchenko, I.N. (2011) X-ray

absorption studies of chlorine valence and local environments in borosilicate waste glasses. Journal of Nuclear Materials, 408 236–245.

Métrich, N., and Rutherford, M.J. (1992) Experimental study of chlorine behavior in hydrous silicic melts. Geochemica et Cosmochimica Acta, 56, 607–616.

Mills, K. (1993) The influence of structure on the physico-chemical properties of slags. The Iron and Steel Institute of Japan International, 33, 148–155.

Millsteed, P.W., and Mavrogenes, J.A. (2015) The discovery of halogens in the ores at Broken Hill, NSW - Economic implications of sulfide melting, 1 p. Canberra.

Moore, G., Vennemann, T., and Carmichael, I.S.E. (1998) An empirical model for the solubility of H2O in magmas to 3 kilobars. American Mineralogist, 83, 36–42.

Moore, W.J., and Nash, J.T. (1974) Alteration and fluid inclusion studies of the porphyry copper ore body at Bingham, Utah. Economic Geology, 69, 631–645.

Mungall, J.E., and Brenan, J.M. (2003) Experimental evidence for the Chalcophile behavior of the halogens. Canadian Mineralogist, 41 207–220.

Nash, T.J. (1976) Fluid-inclusion petrology - Data from porphyry copper deposits and applications to exploration. US Geological Survey Professional Paper, 1–16.

Newman, S., and Lowenstern, J.B. (2002) VOLATILECALC: A silicate melt-H2O-CO2 solution model written in Visual Basic for excel. Computers and Geosciences 28, 597–604.

Nshimiyimana, F., Essarraj, S., and Mohamed, H. (2015) Brines at the Origin of the Silver Mineralization at the Koudia El Hamra Deposit, Central Jebilet, Morocco. In Brines at the origin of the silver mineralization at the Koudia El Hamra deposit, Central Jebilet, Morocco pp. 1–5.

719 Prausnitz, J.M., Lichtenthaler, R.N., and Gomes De Azevedo, E. (1999) Molecular
720 thermodynamics of fluid-phase equilibria, Third., 600 p. (N.R. Amundson, Ed.).
721 Prentice Hall International series in the physical and chemical engineering sciences,
722 New Jersey.

723 Pyle, D.M., and Mather, T.A. (2009) Halogens in igneous processes and their fluxes to the
724 atmosphere and oceans from volcanic activity: A review. Chemical Geology 263, 110–
725 121.

726 Saito, G., Uto, K., Kazahaya, K., Shinohara, H., Kawanabe, Y., and Satoh, H. (2005)
727 Petrological characteristics and volatile content of magma from the 2000 eruption of
728 Miyakejima Volcano, Japan. Bulletin of Volcanology, 67 268–280.

729 Sandland, T.O., Du, L.-S., Stebbins, J.F., and Webster, J.D. (2004) Structure of Cl-containing
730 silicate and aluminosilicate glasses: A 35 Cl MAS-NMR study. Geochimica et
731 Cosmochimica Acta, 68, 5059–5069.

732 Scholtysik, R., and Canil, D. (2021) The effects of S , Cl and oxygen fugacity on the
733 sublimation of volatile trace metals degassed from silicate melts with implications for
734 volcanic emissions. Geochimica et Cosmochimica Acta, In Press.

735 Shannon, R.D. (1976) Revised effective ionic radii and systematic studies of interatomie
736 distances in halides and chaleogenides. Acta Crystallographica, 32, 751–767.

737 Shannon, R.D., and Prewitt, C.T. (1969) Effective ionic radii in oxides and fluorides. Acta
738 Crystallographica Section B Structural Crystallography and Crystal Chemistry 25, 925–
739 946.

740 Sharp, Z.D., and Draper, D.S. (2013) The chlorine abundance of Earth: Implications for a
741 habitable planet. Earth and Planetary Science Letters, 369–370, 71–77.

742 Shinohara, H., Iiyama, J.T., and Matsuo, S. (1989) Partition of chlorine compounds between
743 silicate melt and hydrothermal solutions: I. Partition of NaCl-KCl. Geochimica et
744 Cosmochimica Acta, 53 2617–2630.

745 Signorelli, S., and Carroll, M.R. (2000) Solubility and fluid-melt partitioning of Cl in hydrous
746 phonolitic melts. Geochimica et Cosmochimica Acta, 64 2851–2862.

747 ——— (2002) Experimental study of Cl solubility in hydrous alkaline melts: constraints on
748 the theoretical maximum amount of Cl in trachytic and phonolitic melts. Contributions
749 to Mineral Petrology, 143 209–218.

750 Smith, M.P., Gleeson, S.A., and Yardley, B.W.D. (2013) Hydrothermal fluid evolution and
751 metal transport in the Kiruna District, Sweden: Contrasting metal behaviour in aqueous
752 and aqueous-carbonic brines. Geochimica et Cosmochimica Acta, 102, 89–112.

753 Spilliaert, N., Métrich, N., and Allard, P. (2006) S-Cl-F degassing pattern of water-rich alkali
754 basalt: Modelling and relationship with eruption styles on Mount Etna volcano. Earth
755 and Planetary Science Letters 248, 772–786.

756 Stanley, B.D., Hirschmann, M.M., and Withers, A.C. (2011) CO2 solubility in Martian
757 basalts and Martian atmospheric evolution. Geochimica et Cosmochimica Acta, 75,
758 5987–6003.

759 Stebbins, J.F., and Du, L.-S. (2002) Chloride ion sites in silicate and aluminosilicate glasses:
760 A preliminary study by 35Cl solid-state NMR. American Mineralogist, 87, 359–363.

761 Stelling, J., Botcharnikov, R.E., Beermann, O., and Nowak, M. (2008) Solubility of H 2 O-
762 and chlorine-bearing fluids in basaltic melt of Mount Etna at T = 1050-1250 °C and P =
763 200 MPa. Chemical Geology 256, 101–109.

764 Symonds, R.B., Reed, M.H., and Rose, W.I. (1992) Origin, speciation, and fluxes of trace-

element gases at Augustine volcano, Alaska: insights into magma degassing and fumarolic processes. Geochimica et Cosmochimica Acta, 56, 633–657.

Symonds, R.B., Rose, W.I., Bluth, G.J.S., and Gerlach, T.M. (1994) Volcanic-gas studies: methods, results and applications. In M.R. Carroll and J.R. Holloway, Eds., Reviews in Mineralogy and Geochemistry Vol. 30, pp. 1–66.

Thomas, R.W., and Wood, B.J. (2021) The chemical behaviour of chlorine in silicate melts. Geochimica et Cosmochimica Acta 294 28–42.

von Glasow, R., Bobrowski, N., and Kern, C. (2009) The effects of volcanic eruptions on atmospheric chemistry. Chemical Geology 263, 131–142.

Webster, J.D. (1992) Fluid-melt interactions involving Cl-rich granites: Experimental study from 2 to 8 kbar. Geochimica et Cosmochimica Acta, 56, 659–678.

Webster, J.D., and De Vivo, B. (2002) Experimental and modeled solubilities of chlorine in aluminosilicate melts, consequences of magma evolution, and implications for exsolution of hydrous chloride melt at Mt. Somma-Vesuvius. American Mineralogist, 87, 1046–1061.

Webster, J.D., and Rebbert, C.R. (1998) Experimental investigation of H2O and Cl-solubilities in F-enriched silicate liquids; implications for volatile saturation of topaz rhyolite magmas. Contributions to Mineralogy and Petrology, 132, 198–207.

Webster, J.D., Kinzler, R.J., and Mathez, E.A. (1999) Chloride and water solubility in basalt and andesite melts and implications for magmatic degassing. Geochimica et Cosmochimica Acta, 63, 729–738.

Webster, J.D., Sintoni, M.F., and De Vivo, B. (2009) The partitioning behavior of Cl, S, and H2O in aqueous vapor- ±saline-liquid saturated phonolitic and trachytic melts at

200 MPa. Chemical Geology 263, 19–36.

Webster, J.D., Vetere, F., Botcharnikov, R.E., Goldoff, B., McBirney, A., and Doherty, A.L. (2015) Experimental and modeled chlorine solubilities in aluminosilicate melts at 1 to 7000 bars and 700 to 1250 °c: Applications to magmas of Augustine Volcano, Alaska. American Mineralogist, 100, 522–535.

Webster, J.D., Baker, D.R., and Aiuppa, A. (2018) Halogens in Mafic and Intermediate-Silica Content Magmas. In D.E. Harlov and L. Aranovich, Eds., The Role of Halogens in Terrestrial and Extraterrestrial Geochemical Processes pp. 307–430. Springer Geochemistry.

Webster, J.D., Iveson, A.A., Rowe, M.C., and Webster, P.M. (2019) Chlorine and felsic magma evolution: Modeling the behavior of an under-appreciated volatile component. Geochimica et Cosmochimica Acta 248–288.

Wilkinson, J.J. (2013) Triggers for the formation of porphyry ore deposits in magmatic arcs. Nature Geoscience, 6, 917–925.

Zajacz, Z., Candela, P.A., Piccoli, P.M., and Sanchez-Valle, C. (2012) The partitioning of sulfur and chlorine between andesite melts and magmatic volatiles and the exchange coefficients of major cations. Geochimica et Cosmochimica Acta, 89, 81–101.

Zimova, M., and Webb, S. (2006) The effect of chlorine on the viscosity of Na2O-Fe2O3-Al2O3-SiO2 melts. American Mineralogist, 91, 344–352.

FIGURE CAPTIONS

FIGURE 1. A schematic showing the form of the relationship between the Cl content and the Cl_2 fugacity established by Thomas and Wood (2021). The size of the Henry's Law region depends on the major element composition.

FIGURE 2. Back-Scattered Electron (BSE) image of a typical experimental product, which displays (i) separate and distinct phases of the silicate glass, metal chloride/iodide, and metal and (ii) the CO_2 source as Ag_2CO_3.

FIGURE 3. This figure illustrates the minimum lengths of the Henry's Law, linear regions for melts of different bulk composition at 1.5 GPa/1400^{o}C. It also implies that SiO_2 and CaO contents are likely important parameters in determining Cl solubility, as reflected in our fit for equation (12).

FIGURE 4. Chloride capacity data at 1.5GPa/1400^{o}C plotted against some of the more relevant empirical parameters which aim to describe the degree of polymerisation and acid-base behaviour of silicate melts. See text for definitions and discussion.

FIGURE 5. The expected losses of Cl as HCl from ascending magmas of different composition. All 4 melts were assumed to contain 2000 ppm Cl initially and to begin losing HCl at 50 MPa during isothermal ascent. In all 4 cases the fraction lost, as the surface is approached, varies dramatically with composition where Rhyolite > Dacite > Andesite > Basalt.

831

832 **FIGURE 6.** The calculated Cl contents of the same 4 compositions as in Figure 5 as a
833 function of the NaCl activity at 200 MPa and 900 °C. For a fixed NaCl activity the basalt is
834 calculated to contain ~8 times as much Cl as the rhyolite.

This is the peer-reviewed, final accepted version for American Mineralogist, published by the Mineralogical Society of America.
The published version is subject to change. Cite as Authors (Year) Title. American Mineralogist, in press.
DOI: https://doi.org/10.2138/am-2022-8450. http://www.minsocam.org/

Table 1. Silicate melt compositions used for measuring chlorine solubility

Composition	SiO_2	TiO_2	Al_2O_3	FeO_T	MnO
Icelandic basalt[a]	50.76	1.02	15.32	9.61	-
SM-Basalt[b]	40.76	-	10.52	16.25	-
MORB[c]	50.80	0.82	15.38	7.85	-
Low-Mg Basalt[d]	49.22	3.15	15.82	9.05	0.21
High-Mg Basalt[e]	42.51	4.10	9.54	13.16	0.18
CNMAS ($Fo_5Di_{48}An_{47}$)[f]	48.06	-	16.49	-	-
CNMAS-2 ($En_{17}An_{43}Di_{40}$)[g]	49.61	-	15.36	-	-
CMAS ($An_{50}Di_{28}Fo_{22}$)[h]	46.53	-	18.33	-	-
Lunar Basalti	41.00	9.00	12.00	18.30	0.40
Martian basalt[j]	51.01	1.01	10.15	18.36	0.36
HED-Basalt-1[k]	51.09	-	5.23	15.45	0.10
HED Basalt-2[k]	52.39	0.02	6.67	15.41	0.08
Basanite[l]	45.14	2.47	11.33	12.22	0.19
Andesite[m]	62.85	0.62	18.30	4.01	-
High-Mg Andesite[n]	54.20	0.60	15.60	6.70	-
Dacite[o]	67.22	0.94	15.82	4.47	0.06
Obsidian[p]	74.35	-	12.87	1.51	0.07
Picrite[q]	49.06	2.01	9.41	11.30	0.17
Nephelinite[r]	43.78	2.42	15.32	10.44	0.31
Syn-Nephelinite[s]	39.95	2.76	13.50	11.79	0.28
Phonolite[t]	55.21	0.34	21.31	2.84	0.26
Syn-phonolite[u]	54.55	1.60	19.09	5.53	0.16
Granite[v]	74.74	-	14.92	-	-
Albite/Forsterite ($Ab_{95}Fo_5$)[w]	69.92	-	18.95	-	-
Syn-Rhyolite-1[o]	75.22	0.29	13.53	1.04	0.05
Rhyolite-2[x]	73.66	0.22	13.45	1.25	0.03

$FeO_T = FeO + Fe_2O_3$

[a]Natural Icelandic Basalt (Norris and Wood, 2017)

[b]Synthetic Basalt (Sossi et al., 2019)

[c]Synthetic Mid Ocean Ridge Basalt (MORB), by Kiseeva and Wood, (2013) based on Falloon ar

[d]Natural Low-Mg Basalt, El Hierro, Canary Islands, Tephrite, EGT17-01 (Taracsák et al., 2021)

[e]Natural High-Mg Basalt, El Hierro, Canary Islands, Basanite, TNR14-01 (Taracsák et al., 2021

[f]1 bar eutectic compositon (Osborn and Tait, 1952)

[g]1 bar eutectic compositon (Hytonen and Schairer, 1960)

[h]1.5 GPa approximate eutectic composition, (Presnall et al., 1978)

[i]Synthetic Lunar Basalt model from Apollo 11

[j]Synthetic Martian Basalt (Matzen et al., 2022)

[k]Synthetic bulk silicate compositions of Vesta (Ashcroft and Wood, 2015)

[l]Synthetic Basanite, modelled from the Nepheline basanite sample UT-70489 (Adam, 1990)

[m]Synthetic Andesite (Carmichael et al., 1974)

[n]Synthetic High-Mg Andesite (Wood and Turner, 2009)

[o]Dacite and Rhyolite compositons based on STXB4y and STXG4y respectively (Muir et al., 201

[p]Natural Lipari Obsidian LIP-17714 (Hunt and Hill, 1993)

[q]Natural Picrite, Hawaii, HAW-16095 (Taracsák et al., 2021)

[r]Natural Lacher See Nephelinite, LS-17980 (Taracsák et al., 2021)

[s]Syntheric Nephelinite (Webb and Dingwell, 1990)

[t]Natural Laacher See Phonlite, LS-17985 (Taracsák et al., 2021)

[u]Synthetic Phonolite (Ridley, 1970)

[v]Anhydrous granitic eutectic composition (Ebadi and Johannes, 1991)

[w]Synthetic mixture of 95% Albite and 5% Forsterite

[x]Synthetic Rhyolite made from the compositions of (Nockolds., 1954)

MgO	CaO	Na_2O	K_2O	P_2O_5	Cr_2O_3	NiO
9.19	12.26	2.01	-	-	-	-
15.10	16.69	-	-	-	-	-
10.44	12.62	1.37	-	-	-	-
4.20	9.38	4.77	1.99	1.32	-	-
13.46	11.34	2.79	1.05	0.69	-	-
12.30	21.75	0.90	-	-	-	-
14.27	19.25	1.29	-	-	-	-
17.82	17.33	-	-	-	-	-
8.00	10.00	0.60	-	-	-	-
11.94	6.72	-	-	-	-	0.45
22.60	4.60	0.58	-	-	0.57	0.10
15.99	6.33	0.02	-	-	0.17	0.13
13.59	9.82	2.16	0.23	-	-	-
3.49	6.89	3.37	1.04	-	-	-
9.40	9.60	2.60	1.30	-	-	-
1.45	3.40	2.12	4.24	0.27	-	-
0.05	0.74	3.93	5.11	-	-	-
16.99	8.08	1.74	0.37	0.22	-	-
4.25	11.71	5.39	3.79	1.22	-	-
7.86	12.94	4.54	3.32	1.55	-	-
0.12	1.82	8.15	8.56	0.05	-	-
1.76	4.07	9.06	3.64	0.12	-	-
-	-	6.61	3.72	-	-	-
2.85	-	7.30	-	-	-	-
0.22	0.77	2.18	6.60	0.08	-	-
0.32	1.13	2.99	5.35	0.07	-	-

ıd Green, (1987)

)

l)

4)

LOI	Total
	100.17
	99.32
	99.28
	99.11
	98.82
	99.50
	99.78
	100.01
	99.30
	100.00
	100.32
2.79	100.00
2.85	100.00
	100.57
	100.00
	99.99
	98.63
	99.35
	98.63
	98.49
	98.66
	99.58
	99.99
	99.02
	99.98
0.78	99.25

This is the peer-reviewed, final accepted version for American Mineralogist, published by the Mineralogical Society of America.
The published version is subject to change. Cite as Authors (Year) Title. American Mineralogist, in press.
DOI: https://doi.org/10.2138/am-2022-8450. http://www.minsocam.org/

Table 2: Experimental conditions and compositions

Experiment ID	Silicate composition*	Time (hours)	Pressure (GPa)	Temperature (°C)
Ab/Fo-1	95% Albite - 5% Forsterite	1	1.5	1400
Ab/Fo-2	Ab/Fo + $CaCO_3$	1	1.5	1400
Ab/Fo-3	Ab/Fo + $CaCO_3$	1	1.5	1400
Ab/Fo-6	Ab/Fo + $CaCO_3$	1	1.5	1400
AgI/Cl-27†	Icelandic Basalt	1	1.5	1400
AgI/Cl-005†	CMAS	1	1.5	1400
AgI/Cl-024†	CMAS+ FeO	1	1.5	1400
AgI/Cl-025†	CMAS+ FeO	1	1.5	1400
AgI/Cl-026†	CMAS+ FeO	1	1.5	1400
CMAS+Na-1	CMAS + Na_2CO_3	2	1.5	1400
CMAS+Na+2	CMAS + Na_2CO_3	2	1.5	1400
$Fo_5Di_{48}An_{47}$	CNMAS	2	1.5	1400
$En_{17}An_{43}Di_{40}$	CNMAS-2	2	1.5	1400
Dacite-1	Dacite	2	1.5	1400
Dacite-2	Dacite	1	1.5	1400
TNR14-1	High Mg Basalt	1	1.5	1400
HA3-2	Basalt	2	1.5	1400
HA4-1	Basalt	1	1.5	1400
Rhyolite	Rhyolite	1	1.5	1400
LIP-17714	Lipari Obsidian	1	1.5	1400
AN-1	Andesite	4	1.5	1400
AN-2	Andesite	2	1.5	1400
SM-1	Basalt	2	1.5	1400
HiMgAnd	Andesite	1	1.5	1400
HAW-16095	Picrite	1	1.5	1400
EGT17-1	Low Mg Basalt	1	1.5	1400
KK3b-1	MORB	1	1.5	1400
KK3b-2	MORB	1	1.5	1400
Mars-1	Martian Basalt	1	1.5	1400
LS-17980	Nephelinite	1	1.5	1400
Basanite-1	Basanite	2	1.5	1400
Lunar-1	Lunar basalt	2	1.5	1400
KK-Rhy	Rhyolite	2	1.5	1400
Syn-Phono-1	Syn-Phonolite	2	1.5	1400
LS-17985-1	Phonolite	2	1.5	1400

LS-17985-2	Phonolite	2	1.5	1400
Granite-2	Granite	2	1.5	1400
Gran+Mg-1	Granite + MgO	2	1.5	1400
Gran+Mg-2	Granite + MgO	2	1.5	1400
Gran+Mg-3	Granite + MgO	2	1.5	1400
Phonolite-NaCl-1§	80% LS-17985; 20% NaCl	0.5	1.0	1100
Phonolite-NaCl-2§	80% LS-17985; 20% NaCl	2	1.0	1100
Time series				
Dacite-3	Dacite	0.75	1.5	1400
Dacite-4	Dacite	0.083	1.5	1400

Cl% error in () is 2 stdev

*Starting silicate melt compositions presented in Table 1

† Experiments originally presented in Thomas and Wood, (2021)

§ $f(Cl_2)$ and C_{Cl} calculated using *ChlorCalc_v1* (Spreadsheet available in the supplementa

C_{Cl} = Chloride capacity, OB = Optical Basicity, IP = Ionic Porosity, LI = Larsen Index (see

This is the peer-reviewed, final accepted version for American Mineralogist, published by the Mineralogical Society of America.
The published version is subject to change. Cite as Authors (Year) Title. American Mineralogist, in press.
DOI: https://doi.org/10.2138/am-2022-8450. http://www.minsocam.org/

Measured Cl^{glass} wt%	Buffer/Silicate by mass	AgI/AgCl	Final Molar *Cl/(Cl+I)*	Molar *Ag/(Ag+Pt)*	$f(O_2)$ *buffer*	*log* $f(O_2)$
0.56 (0.02)	75/25	75/25	0.325	0.879	CCO	-7.17
1.41 (0.06)	75/25	75/25	0.276	0.943	CCO	-7.17
2.75 (0.05)	75/25	75/25	0.183	0.812	CCO	-7.17
0.46 (0.01)	80/20	75/25	0.123	0.892	CCO	-7.17
1.6 (0.03)	50/50	75/25	0.209	0.778	CCO	-7.17
2.55 (0.04)	75/25	75/25	0.198	0.844	CCO	-7.17
2.54 (0.06)	75/25	75/25	0.198	0.887	CCO	-7.17
2.70 (0.19)	75/25	75/25	0.184	0.864	CCO	-7.17
3.49 (0.28)	75/25	75/25	0.120	0.903	CCO	-7.17
2.15 (0.06)	75/25	75/25	0.227	0.800	CCO	-7.17
2.32 (0.1)	75/25	75/25	0.214	0.836	CCO	-7.17
2.41 (0.14)	75/25	75/25	0.208	0.937	CCO	-7.17
2.60 (0.13)	75/25	75/25	0.194	0.793	CCO	-7.17
0.46 (0.08)	75/25	75/25	0.332	0.854	CCO	-7.17
0.17 (0.01)	75/25	90/10	0.142	0.776	CCO	-7.17
2.23 (0.12)	75/25	75/25	0.221	0.913	CCO	-7.17
1.62 (0.16)	75/25	75/25	0.265	0.882	CCO	-7.17
1.75 (0.2)	75/25	75/25	0.254	0.858	CCO	-7.17
0.27 (0.03)	75/25	75/25	0.340	0.812	CCO	-7.17
0.27 (0.03)	75/25	75/25	0.340	0.832	CCO	-7.17
0.72 (0.03)	25/75	75/25	0.227	0.785	CCO	-7.17
0.90 (0.05)	75/25	75/25	0.306	0.893	CCO	-7.17
3.05 (0.16)	75/25	75/25	0.158	0.938	CCO	-7.17
1.71 (0.03)	75/25	75/25	0.257	0.916	CCO	-7.17
1.90 (0.14)	75/25	75/25	0.244	0.947	CCO	-7.17
1.40 (0.02)	75/25	75/25	0.276	0.837	CCO	-7.17
1.13 (0.02)	25/75	75/25	0.130	0.707	CCO	-7.17
1.70 (0.04)	75/25	75/25	0.257	0.754	CCO	-7.17
2.02 (0.2)	75/25	75/25	0.236	0.961	CCO	-7.17
1.91 (0.03)	75/25	75/25	0.244	0.906	CCO	-7.17
2.06 (0.03)	75/25	75/25	0.234	0.897	CCO	-7.17
2.03 (0.09)	75/25	75/25	0.235	0.935	CCO	-7.17
0.15 (0.02)	75/25	75/25	0.347	0.948	CCO	-7.17
0.83 (0.02)	75/25	75/25	0.310	0.764	CCO	-7.17
0.68 (0.07)	75/25	75/25	0.319	0.955	CCO	-7.17

This is the peer-reviewed, final accepted version for American Mineralogist, published by the Mineralogical Society of America.
The published version is subject to change. Cite as Authors (Year) Title. American Mineralogist, in press.
DOI: https://doi.org/10.2138/am-2022-8450. http://www.minsocam.org/

0.44 (0.03)	75/25	90/10	0.170	0.943	CCO	-7.17
0.31 (0.10)	75/25	75/25	0.339	0.916	CCO	-7.17
0.61 (0.10)	75/25	75/25	0.323	0.770	CCO	-7.17
0.67 (0.14)	75/25	75/25	0.320	0.918	CCO	-7.17
0.78 (0.10)	75/25	75/25	0.313	0.844	CCO	-7.17
1.09 (0.10)	-	-	-	-	RRO	-6.77
1.00 (0.12)	-	-	-	-	CCO	-10.31
0.47 (0.06)	75/25	75/25	0.330	0.856	CCO	-7.17
0.50 (0.17)	75/25	75/25	0.329	0.854	CCO	-7.17

ry)

text). RRO=Re/ReO2 buffer

$f(Cl_2)$	C_{Cl}	OB	NBO/T	IP	LI
8.08E-04	0.32	0.53	0.00	72.56	20.66
5.05E-04	1.01	0.56	0.27	71.12	8.01
2.98E-04	2.57	0.58	0.57	69.81	-2.88
1.12E-04	0.70	0.58	0.38	70.54	5.54
4.24E-04	1.25	0.58	0.57	69.60	-5.10
3.24E-04	2.29	0.60	0.94	67.24	-18.22
2.94E-04	2.39	0.61	1.09	66.95	-23.01
2.68E-04	2.66	0.62	1.21	66.86	-25.94
1.04E-04	5.52	0.64	1.56	65.72	-34.06
4.76E-04	1.59	0.61	1.03	67.79	-13.33
3.89E-04	1.90	0.61	0.99	67.33	-17.34
2.92E-04	2.28	0.60	0.89	67.66	-16.97
3.52E-04	2.24	0.60	1.00	67.72	-16.44
8.90E-04	0.25	0.53	0.01	72.86	22.14
1.98E-04	0.20	0.53	0.00	73.03	23.44
3.47E-04	1.93	0.60	1.14	68.79	-18.68
5.32E-04	0.67	0.59	1.50	67.19	-23.23
5.18E-04	1.24	0.58	0.93	68.71	-9.84
1.04E-03	0.14	0.52	0.00	73.51	30.83
9.85E-04	0.14	0.52	0.00	73.49	29.18
4.92E-04	0.52	0.55	0.15	71.76	13.02
6.93E-04	0.55	0.55	0.15	71.72	11.17
1.67E-04	3.81	0.62	1.51	66.32	-28.16
4.65E-04	1.28	0.58	0.58	69.72	-4.45
3.93E-04	1.55	0.59	0.88	69.27	-12.20
6.43E-04	0.89	0.57	0.28	71.59	5.24
2.00E-04	1.29	0.59	0.72	69.45	-10.45
6.88E-04	1.05	0.58	0.57	69.45	-5.74
3.57E-04	1.73	0.60	1.14	68.09	-20.24
4.27E-04	1.49	0.60	0.62	69.64	-9.56
4.00E-04	1.66	0.59	0.93	68.96	-12.73
3.75E-04	1.69	0.60	0.78	70.90	-14.80
7.91E-04	0.09	0.52	0.00	73.28	27.25
9.72E-04	0.43	0.55	0.07	72.20	16.79
6.61E-04	0.43	0.56	0.00	72.06	21.84

1.92E-04	0.51	0.57	0.02	71.93	21.01
8.08E-04	0.18	0.52	0.00	73.32	28.08
1.04E-03	0.31	0.54	0.10	72.34	20.89
7.16E-04	0.40	0.54	0.15	72.09	19.03
8.09E-04	0.44	0.54	0.20	71.71	16.31
2.70E-03	0.42	0.57	0.00	72.67	21.28
4.46E-05	0.40	0.57	0.01	72.59	19.39
8.78E-04	0.26	-	-	-	-
8.77E-04	0.27	-	-	-	-

Table 3. Normalised silicate melt compositions at water saturation

Composition	Temperature (°C)	SiO_2	TiO_2	Al_2O_3	FeO_T	MnO	MgO	CaO
Icelandic basalt	1220	49.57	1.00	14.96	9.38	-	8.97	11.97
Andesite	1200	61.16	0.61	17.81	3.91	-	3.40	6.70
Dacite	1080	65.72	0.92	15.47	4.37	0.06	1.42	3.32
Rhyolite	1030	73.48	0.28	13.21	1.02	0.05	0.21	0.75

*H_2O contents are calculated from Moore et al., (1998) at 50 Mpa, using anhydrous compositions (Tab

Na_2O	K_2O	P_2O_5	H_2O*	Total
1.97	-	-	2.18	100.00
3.28	1.01	-	2.13	100.00
2.07	4.15	0.26	2.24	100.00
2.13	6.45	0.08	2.34	100.00

ɔle 1)

Fig 1

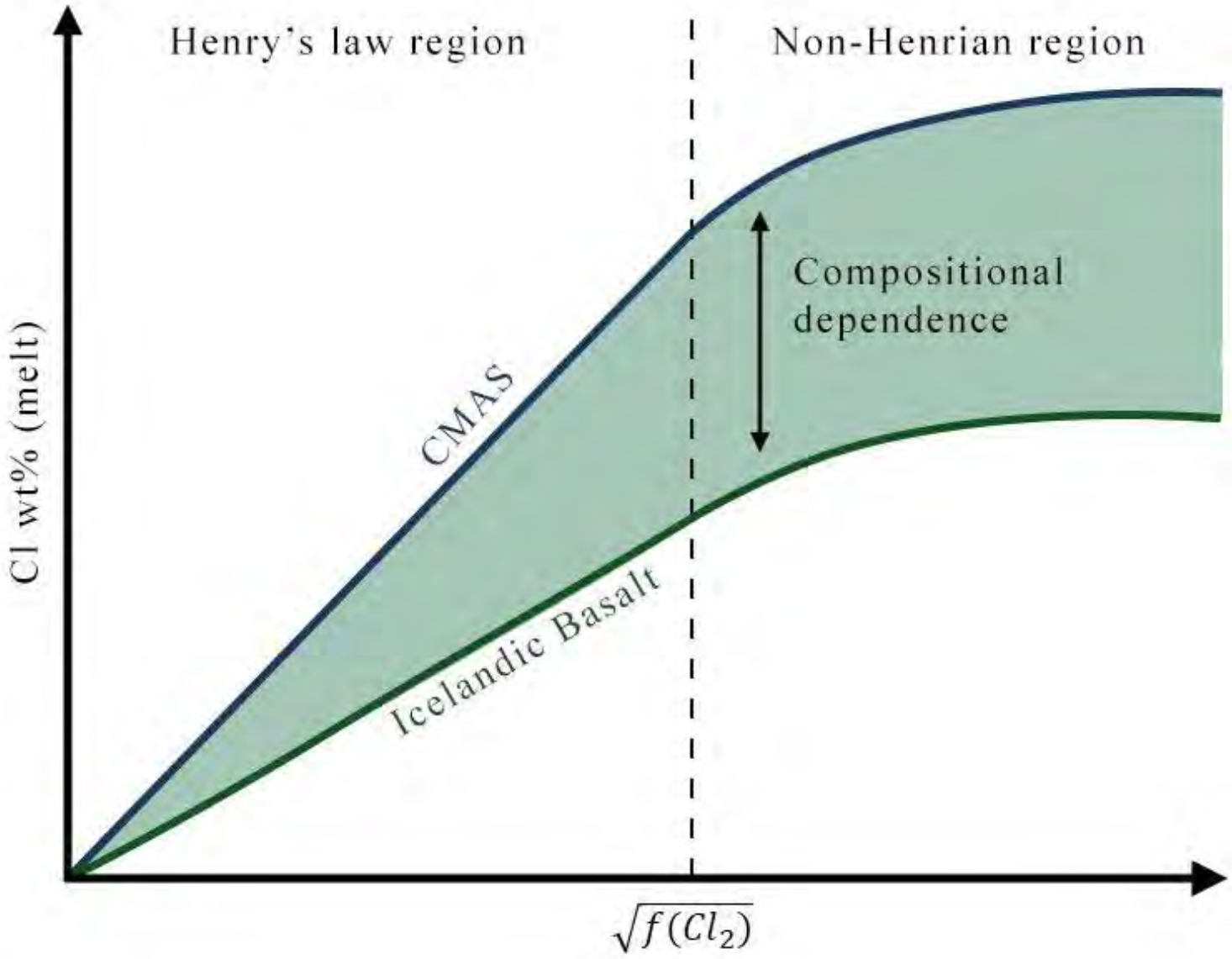

This is the peer-reviewed, final accepted version for American Mineralogist, published by the Mineralogical Society of America.
The published version is subject to change. Cite as Authors (Year) Title. American Mineralogist, in press.
DOI: https://doi.org/10.2138/am-2022-8450. http://www.minsocam.org/

Fig 2

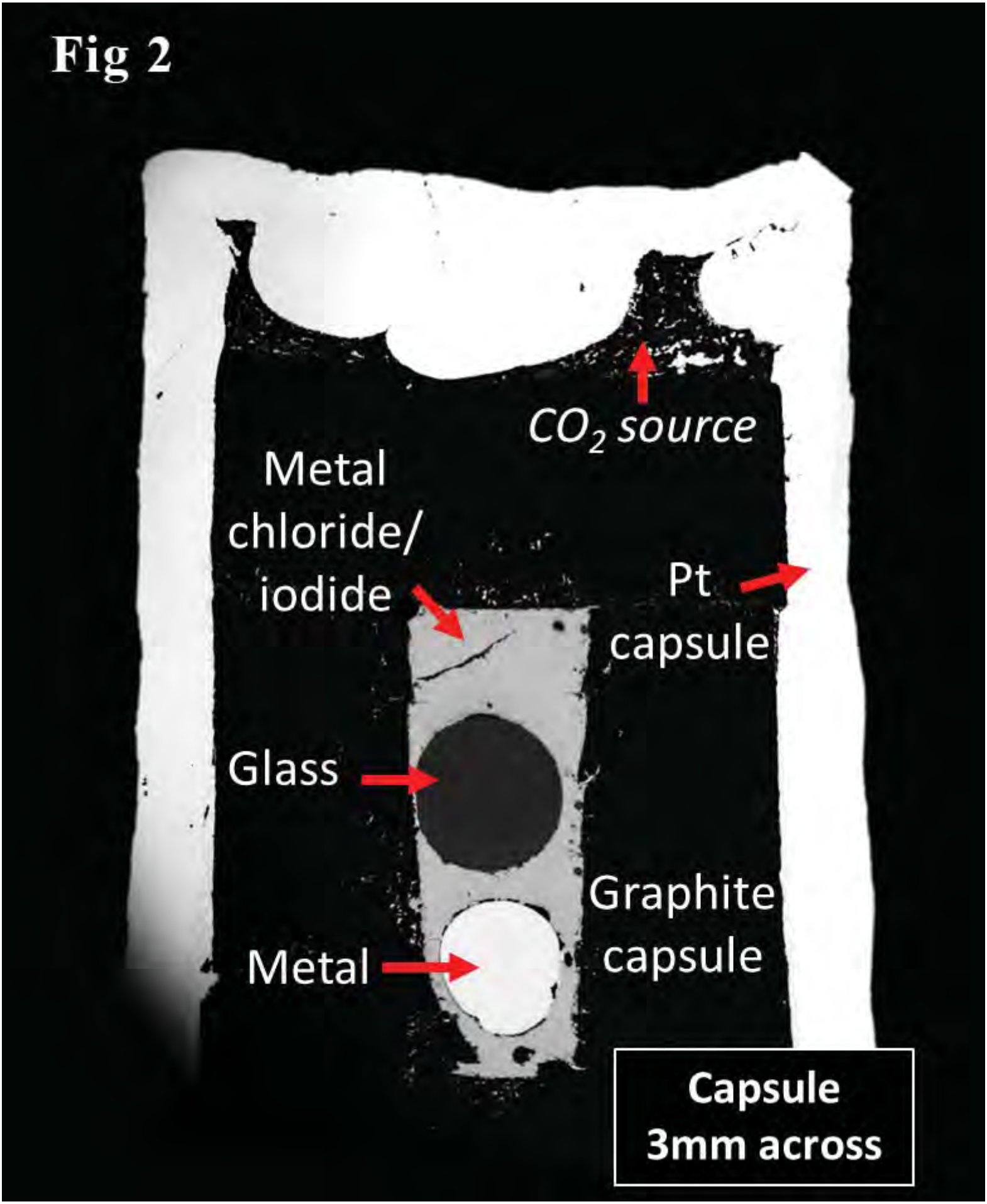

This is the peer-reviewed, final accepted version for American Mineralogist, published by the Mineralogical Society of America.
The published version is subject to change. Cite as Authors (Year) Title. American Mineralogist, in press.
DOI: https://doi.org/10.2138/am-2022-8450. http://www.minsocam.org/

Fig 3

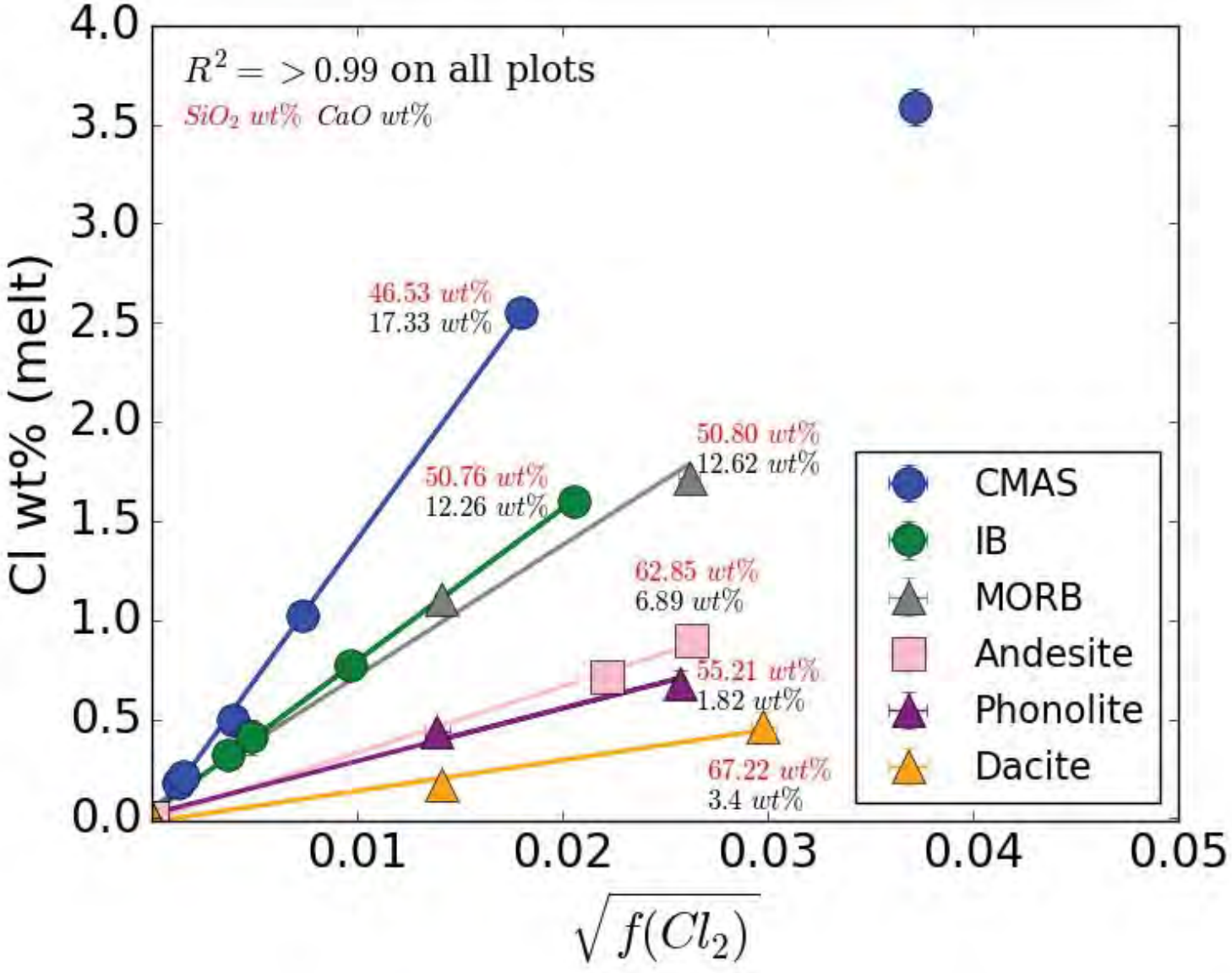

This is the peer-reviewed, final accepted version for American Mineralogist, published by the Mineralogical Society of America.
The published version is subject to change. Cite as Authors (Year) Title. American Mineralogist, in press.
DOI: https://doi.org/10.2138/am-2022-8450. http://www.minsocam.org/

Fig 4

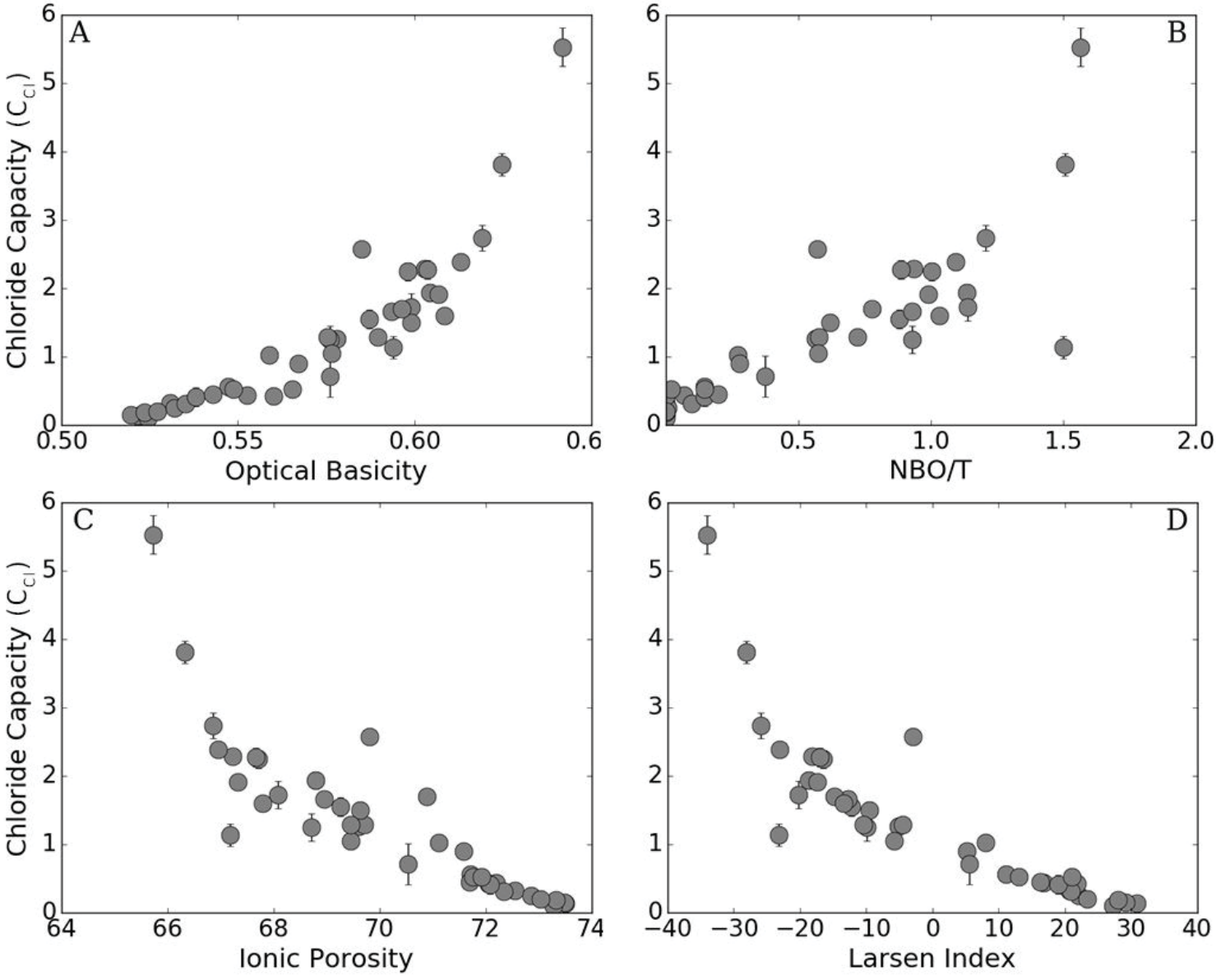

Fig 5

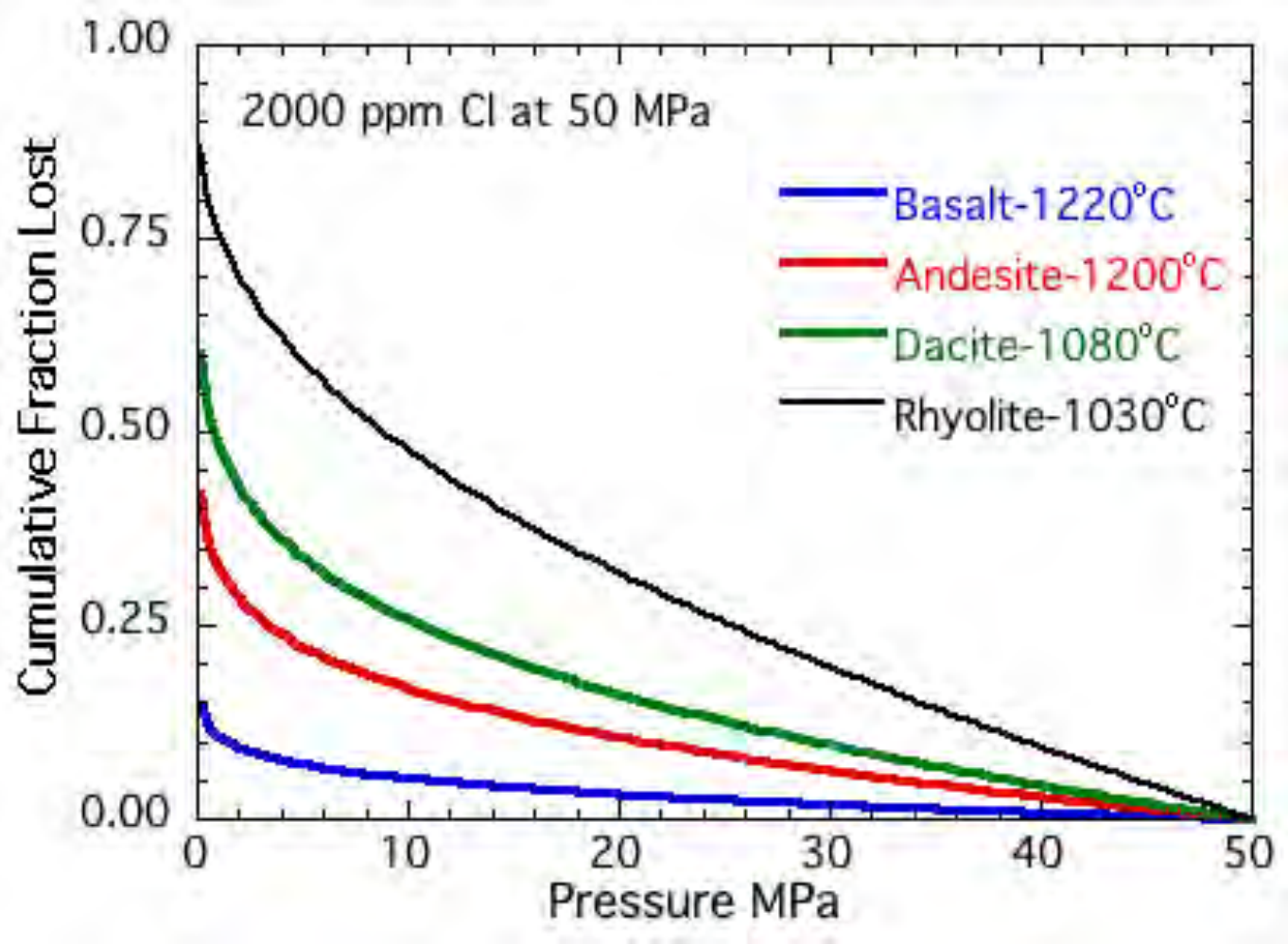

Fig 6